AD-A193 125 THE STRUCTURES OF SELF-ASSEMBLED MONOLAYER FILMS OF ORGANOSULFUR COMPOUND..(U) HARVARD UNIV CAMBRIDGE MASS DEPT OF CHEMISTRY L STRONG ET AL. JAN 88 TR-4 1/1

UNCLASSIFIED N00014-85-K-0098 F/G 7/4 NL

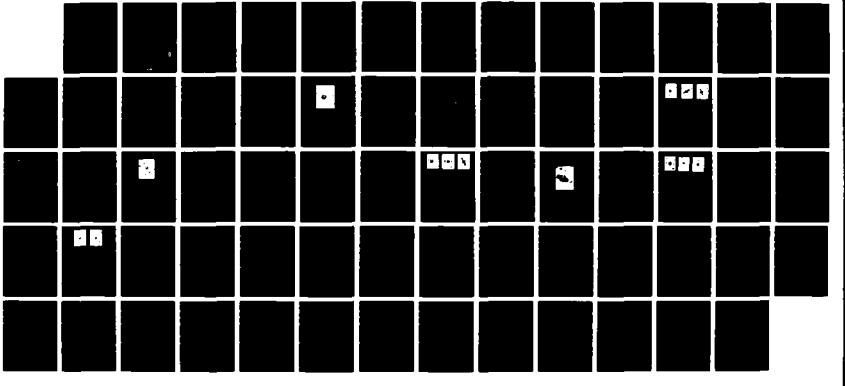

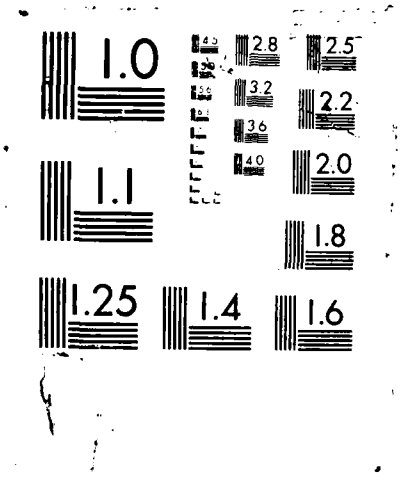
1.0
1.1
1.25
1.4
1.6
1.8
2.0
2.2
2.5
2.8
3.2
3.6
4.0

AD-A193 125

(4)

THE STRUCTURES OF SELF-ASSEMBLED MONOLAYER FILMS OF ORGANOSULFUR COMPOUNDS ADSORBED ON GOLD SINGLE CRYSTALS: ELECTRON DIFFRACTION STUDIES

Lou Strong and George M. Whitesides*
Department of Chemistry
Harvard University
Cambridge MA 02138

DTIC FILE COPY

Technical Report No. 4 (January 1988)

Interim Technical Report (Accepted for publication in Langmuir)

PREPARED FOR DEFENSE ADVANCED RESEARCH PROJECTS AGENCY
1400 Wilson Boulevard
Arlington VA 22209

DEPARTMENT OF THE NAVY
Office of Naval Research, Code 1130P
800 North Quincy Street
Arlington VA 22217-5000

ARPA Order No.: NR 356-856
Contract No.: N00014-85-K-0898
Effective Date: 85 September 01
Expiration Date: 88 August 31

DTIC ELECTE MAR 28 1988 S D C&E

Principal Investigator: George M. Whitesides
(617) 495-9430

The views and conclusions in this document are those of the authors and should not be interpreted as necessarily representing the official policies, either expressed or implied, of the Defense Advanced Research Projects Agency or the U.S. Government.

This document has been approved for public release and sale; its distribution is unlimited.

REPRODUCED AT GOVERNMENT EXPENSE

SECURITY CLASSIFICATION OF THIS PAGE

REPORT DOCUMENTATION PAGE

1a. REPORT SECURITY CLASSIFICATION Unclassified	1b. RESTRICTIVE MARKINGS
2a. SECURITY CLASSIFICATION AUTHORITY	3. DISTRIBUTION / AVAILABILITY OF REPORT Approved for public release; distribution unlimited
2b. DECLASSIFICATION / DOWNGRADING SCHEDULE	
4. PERFORMING ORGANIZATION REPORT NUMBER(S) Technical Report #4	5. MONITORING ORGANIZATION REPORT NUMBER(S)
6a. NAME OF PERFORMING ORGANIZATION Harvard University 6b. OFFICE SYMBOL (*If applicable*)	7a. NAME OF MONITORING ORGANIZATION Office of Naval Research
6c. ADDRESS (*City, State, and ZIP Code*) Office for Sponsored Research Holyoke Center, Fourth Floor Cambridge MA 02138-4993	7b. ADDRESS (*City, State, and ZIP Code*) Code 11130P 800 North Quincy Street Arlington VA 22217-5000
8a. NAME OF FUNDING / SPONSORING ORGANIZATION ONR/DARPA 8b. OFFICE SYMBOL (*If applicable*)	9. PROCUREMENT INSTRUMENT IDENTIFICATION NUMBER
8c. ADDRESS (*City, State, and ZIP Code*) 800 North Quincy Street Arlington VA 22217-5000	10 SOURCE OF FUNDING NUMBERS PROGRAM ELEMENT NO. 85-K-0898 / PROJECT NO. NR 356-856 / TASK NO / WORK UNIT ACCESSION NO

11 TITLE (*Include Security Classification*)
The Structures of Self-Assmebled Monolayer Films of Organosulfur Compounds Adsorbed on Gold Single Crystals: Electron Diffraction Studies

12. PERSONAL AUTHOR(S) Lou Strong and George M. Whitesides

13a. TYPE OF REPORT	13b. TIME COVERED	14. DATE OF REPORT (*Year, Month, Day*)	15. PAGE COUNT
Interim	FROM _____ TO _____	January 1988	

16. SUPPLEMENTARY NOTATION

17. COSATI CODES			18. SUBJECT TERMS (*Continue on reverse if necessary and identify by block number*)
FIELD	GROUP	SUB-GROUP	gold, monolayer, electron diffraction, thin film, structure, self-assembly

19. ABSTRACT (*Continue on reverse if necessary and identify by block number*)

Transmission electron microscopy and diffraction have been used to study the packing arrangements of docosyl thiol ($CH_3(CH_2)_{21}SH$, RSH), didocosyl sulfide (RSR), and didocosyl disulfide (RSSR) on gold single crystal foils. The specimens include gold films in (100) and (111) orientations. Docosyl thiol and didocosyl disulfide adsorbed on (111) faces assemble in coincidence lattice structures yielding hexagonal overlayers c(7 x 7) in which the short interchain distance (4.97 Å) indicates freely rotating methylene chains. On a (100) surface both alkyl groups exhibit an in-plane structure consisting of a base-centered square array in which the interchain distance (4.54 Å) implies a hindered chain movement. The spacing here is a rational multiple (10/9) of the sublattice spacing, suggesting that the overlayer is repeated in the center lattice c(10 x 10). Although docosyl thiol and didocosyl disulfide present the

20 DISTRIBUTION / AVAILABILITY OF ABSTRACT ☒ UNCLASSIFIED/UNLIMITED ☐ SAME AS RPT ☐ DTIC USERS	21 ABSTRACT SECURITY CLASSIFICATION
22a NAME OF RESPONSIBLE INDIVIDUAL Dr. Kenneth J. Wynne	22b TELEPHONE (*Include Area Code*) / 22c OFFICE SYMBOL

DD FORM 1473, 84 MAR 83 APR edition may be used until exhausted
All other editions are obsolete

SECURITY CLASSIFICATION OF THIS PAGE

19. Abstract (cont'd)

same in-plane structures on a (111) surface, on a (100) surface the dialkyl disulfide exhibits additional phases as well. These phases are incommensurate with the predominant subsurface (100) lattice; however, the interchain spacings indicate that they are repeated in the base-centered square overlayers c(7/2 $\sqrt{2}$ x 7/2 $\sqrt{2}$) and c(5 x 5). Their translational correlation lengths are greater than the correlation lengths of the hexagonal overlayer and the c(10 x 10) square overlayer, but the orientational correlations are similar and are long-range in all phases. Measurements of the diffraction intensity and spot displacement with sample tilting indicate that thiol and disulfide chain inclination has a probability distribution that is axially symmetric about the vector normal to either substrate. The measurement of the average chain inclination from the falloff of diffracted beam intensity with beam tilt is complicated by anomalous attentuation associated with dynamical scattering from the substrate. Estimates of tilt angle indicate that the hcp phase has the greatest average tilt (25-35°); this is followed by the c(10 x 10) square overlayer (6-12°) and finally by the c(7/2 $\sqrt{2}$ x 7/2 $\sqrt{2}$) and c(5 x 5) square overlayers (<6°).

The phases of didocosyl sulfide (RSR) on gold are ambiguous. All diffraction data indicate structures that are isomorphous with didocosyl disulfide (RSSR). The weaker binding of the sulfide compared to the disulfide, however, suggests the possibility that adsorbed disulfide impurities may mask the true sulfide phase.

LA8700876
REVISED

The Structures of Self-Assembled Monolayer Films of Organosulfur Compounds Adsorbed on Gold Single Crystals: Electron Diffraction Studies.

Lou Strong* and George M. Whitesides*

Division of Applied Science and
Department of Chemistry
Harvard University
Cambridge, Massachusetts 02139

Accession For
NTIS GRA&I [X]
DTIC TAB [ ]
Unannounced [ ]
Justification
By
Distribution/
Availability Codes
Dist | Avail and/or Special
A-1

Abstract. Transmission electron microscopy and diffraction have been used to study the packing arrangements of docosyl thiol ($CH_3(CH_2)_{21}SH$, RSH), didocosyl sulfide (RSR), and didocosyl disulfide (RSSR) on gold single crystal foils. The specimens include gold films in (100) and (111) orientations. Docosyl thiol and didocosyl disulfide adsorbed on (111) faces assemble in coincidence lattice structures yielding hexagonal overlayers c(7 x 7) in which the short interchain distance (4.97 Å) indicates freely rotating methylene chains. On a (100) surface both alkyl groups exhibit an in-plane structure consisting of a base-centered square array in which the interchain distance (4.54 Å) implies a hindered chain movement. The spacing here is a rational multiple (10/9) of the sublattice spacing, suggesting

that the overlayer is repeated in the center lattice c(10 x 10). Although docosyl thiol and didocosyl disulfide present the same in-plane structures on a (111) surface, on a (100) surface the dialkyl disulfide exhibits additional phases as well. These phases are incommensurate with the predominant subsurface (100) lattice; however, the interchain spacings indicate that they are repeated in the base-centered square overlayers c(7/2 $\sqrt{2}$ x 7/2 $\sqrt{2}$) and c(5 x 5). Their translational correlation lengths are greater than the correlation lengths of the hexagonal overlayer and the c(10 x 10) square overlayer, but the orientational correlations are similar and are long-range in all phases. Measurements of the diffraction intensity and spot displacement with sample tilting indicate that thiol and disulfide chain inclination has a probability distribution that is axially symmetric about the vector normal to either substrate. The measurement of the average chain inclination from the falloff of diffracted beam intensity with beam tilt is complicated by anomalous attentuation associated with dynamical scattering from the substrate. Estimates of tilt angle indicate that the hcp phase has the greatest average tilt (25-35°); this is followed by the c(10 x 10) square overlayer (6-12°) and finally by the c(7/2 $\sqrt{2}$ x 7/2 $\sqrt{2}$) and c(5 x 5) square overlayers (<6°).

The phases of didocosyl sulfide (RSR) on gold are ambiguous. All diffraction data indicate structures that are isomorphous with didocosyl disulfide (RSSR). The weaker binding of the sulfide compared to the disulfide, however, suggests the pos-

sibility that adsorbed disulfide impurities may mask the true sulfide phase.

Introduction

High resolution electron microscopy and electron diffraction techniques have been used to study the molecular packing of monolayer and multilayer organic films, particularly long alkyl chains of various terminal functionality. Monolayer films have been studied as adsorbates on metallic,[1] semimetallic,[2] and oxide surfaces,[3] and as Langmuir-Blodgett films deposited on amorphous substrates.[4,5] The structure of long paraffin chains in monolamellar and multi-lamellar assemblies has received considerable attention because of their importance as models of biological membrane systems, tunneling barriers for electron and ion transport, and agents for enhancing the wettability, adhesion, lubrication, wear, and passivation of surfaces.

Kitaigorodskii[6] and Segerman[7] have described hydrocarbon chain packing arrangements from single crystal X-ray structure determinations of multi-lamellar paraffin crystals and have compared them with theoretical models based upon van der Waals interaction volumes. The latter fall into three different categories (and four different space groups) depending on whether the hydrocarbon chain axes are all parallel, whether alternate chain layers are crossed, or whether the alkyl chains have rotational symmetry. Examining all possible symmetry relations of a saturated hydrocarbon chain in extended <u>trans</u> configuration

and arbitrary length, Segerman found that ten possible subcells are obtained when all chain axes are parallel and thirty-one when they are not. Of these, six different subcells have so far been observed in the first category and two in the second. The detailed structure(s) of the postulated hexagonal (rotator) phase is not well known, but it is thought to involve translational as well as tilt disorder. Conversion from an orthorhombic unit cell to a hexagonal one has been demonstrated for undecanoic acid by raising the temperature to several degrees below melting.[8]

The strategy underlying the packing analyses was to ignore distortions that occur close to the chain ends where shear may be introduced because end groups do not permit the convex parts along one chain to fit exactly into the concave parts along an adjacent chain. The analyses do not address the possibilities of kink formation in cases where end group functionality may pin the chain centers to fixed positions on a substrate surface, thereby raising the energy of a local trans conformation to favor the introduction of a chain point defect or a kink block.[9] Phase transitions of alkyl chains involving the substitution of an all-trans conformation by gauche conformations at the chain end and gauche-trans-gauche conformations in the body of the chain have been induced by elevating temperature,[10] by varying electrolyte concentrations,[11] and by causing terminal groups to interact with macromolecules.[12] In addition, chain tilt produced by the competition between the spacings preferred by the various head groups and their nonpolar tails[13] becomes increasingly sig-

nificant as hydrocarbon chain lengths decrease.

Recently, interest has turned towards alkyl chains with specific head group functionality that permits adsorption onto specific substrate sites from a solution phase, and the spontaneous assembly of such adsorbates into close-packed, oriented quasi two-dimensional monolayers. Alkyl thiols (RSH) and dialkyl disulfides (RSSR) have been shown to be systems that self-assemble into close-packed alkyl monolayers from solution on gold surfaces.[14] They have been used to promote adhesion between a conducting surface and polyethylene,[15] have been shown to exhibit extraordinary resistance to electron tunneling in the electrochemical reduction of ferricyanide at a coated gold electrode,[16] have been found to alter the grain morphology of thermally deposited gold and silver film on aluminum and silver oxide substrates,[17] and to alter dramatically the wetting properties of evaporated gold films.[18]

The bonding of a sulfide headgroup to a substrate is expected to impart strong bond-oriented ordering in the plane of the film. A model is provided by Oudar et al.,[19] who studied the chemisorption of hydrogen sulfide gas on (100), (111), and (110) faces of gold single crystals under ultra-high vacuum conditions using LEED and Auger spectroscopies. They identified four LEED patterns for the two-dimensional sulfur layer on Au(100). Each exhibited similar square mesh diagrams but different coordination symmetries, desorption temperatures, and inter-sulfide distances. The most stable structure appears at about half-saturation

coverage and conforms to the overlayer p(2 x 2) where the minimum sulfur-sulfur distance is 5.76 Å--twice the separation between Au atoms along a [110] direction. At higher saturation coverage, rotation and contraction of the surface mesh gave LEED evidence of microdomains having the following overlayer structures and spacings: c(2 x 2), d_{ss} = 4.07 Å, p(6 x 6), d_{ss} = 3.80 Å and c(4 x 4), d_{ss} = 3.64 Å. In the most densely packed structure, the sulfur atoms are believed to coordinate with a variable number of atoms and with neighboring sulfur atoms. On the (111) Au face, exposures up to 10^{-2} torr of hydrogen sulfide gives only half saturation coverage as determined by quantitation under the sulfur Auger peak. Diffraction shows a p(1 x 1) array of spots, corresponding to the adsorption of less than half a monolayer of sulfide. Greater coverage could be achieved only by exposure to both H_2 and H_2S. Indistinct structures that were initially formed owing to the high sulfide mobility on this face ultimately crystallized into a complicated saturation structure.

We undertook a series of electron diffraction studies of docosyl thiol ($CH_3(CH_2)_{21}SH$, RSH), didocosyl sulfide (RSR) and didocosyl disulfide (RSSR) adsorbed on crystalline gold surfaces to examine the effect of substituting different head groups as well as the role of substrate symmetry in determining the modes of chain packing. Both transmission and surface reflection experiments were performed in an effort to evaluate in-plane and plane-parallel structures. The latter has not yet revealed any well-defined reflections attributable to the organic sulfides.

Experimental

Materials. Didocosyl disulfide (mp 76-78 °C) was synthesized in these laboratories by Janette Houk and Yu-Tai Tao; didocosyl sulfide (mp 77.3-78.0 °C) and docosyl thiol (mp 46-48 °C) were synthesized by Ernest B. Troughton.[18] ^{1}H NMR spectra of each compound showed no evidence of any impurity. Cyclohexyl mercaptan was purchased from Aldrich (nominal purity 99.9%) and was used without further purification. Hexadecane (Aldrich Chemical Company), which had a nominal purity of 99%, was further purified by slow elution through a column of alumina and stored under nitrogen. All organosulfur compounds were dissolved in either hexadecane or absolute ethanol.

The gold wire used for vacuum evaporations (99.99% purity) was obtained from Alpha Ventron and Engelhardt. Single crystal sodium chloride (NaCl) and barium fluoride were supplied by Optovac, Inc. and cleaved into slices approximately 1-cm^2 x 2-mm thick along the dominant cleavage planes with a razor blade. Mica sheets were separated by forcing distilled water between leaves with a hypodermic syringe. Silicon wafers were obtained in (100) and (111) orientations from Monsanto.

Sample Preparation and Treatment. A variation of the method of Pashley et al.[20] was used to obtain oriented single crystal gold foils. Gold was evaporated from resistively heated tungsten boats onto cleaved surfaces of NaCl (100) orientation and BaF_2(111) orientation held at a temperature of 300 °C. The deposition was carried out at 10^{-5} to 10^{-6} torr in an oil

diffusion pumped system equipped with a liquid nitrogen trap assembly. After 600-800 Å of gold had been deposited, the temperature was slowly raised to 450 °C and subsequently lowered to ambient temperature at a rate of about 100 °C h^{-1}. Initially, a preevaporated layer of silver was used to try to reduce the deposited thickness of gold necessary to produce a continuous crystalline foil. Our hope was subsequently to dissolve this preevaporated layer in 0.1 N nitric acid. Auger analysis of the acid-treated foils showed, however, that the silver could never be completely removed from either surface of the foil, and we concluded that trace amounts of silver had alloyed with the gold. This surface contamination precluded the use of silver for minimizing foil thickness. Oriented crystalline foils to be used in TEM studies were removed from their substrates by dissolving the substrates in distilled, deionized water.

To avoid possible interference by absorption of surface contaminants, the single crystal foils were electrochemically cleaned by cycling through potentials between +1.5 V (NHE) and -0.4 V (NHE) where gold dissolution is essentially avoided.[21] The apparatus to accomplish this cycling consisted of an electrochemical cell containing 0.1 N $HClO_4$ as electrolyte and gold working and control electrodes. The reference electrode was a double-junction Na_2SO_4/Ag-AgCl electrode, selected to reduce chloride ion contamination. The single crystal gold foils were floated onto 3-mm polycrystalline gold mesh electron microscope grids. A grid containing the sample substrate was sandwiched

between two gold foil covers, each cover having a 2-mm perforation to permit contact of electrolyte with the sample. The foil ccntaining the crystalline sample was connected as the working electrode in a cyclic voltammetry configuration. The voltammetry cell was perfused with argon. After 10-15 min of potential cycling--an interval sufficient to produce a clean surface voltammogram of polycrystalline gold[22]--the sample was removed from the cell, twice rinsed in distilled, deionized water and finally in ethanol. The sample was immersed in a solution containing the desired adsorbate and left for at least 2 h; presumably both faces of the foil were covered with the adsorbate. Ethanol was found to be the better solvent for the adsorption because it did not cause curling of the sample foil. Adsorption was carried out at 25 °C from solutions that had been made slightly supersaturated by warming to about 35-40 °C. Final rinsing was done in absolute ethanol or in hexadecane followed by reagent grade hexane.

The effectiveness of this procedure in producing close-packed organic monolayer films was judged by parallel voltametric and ellipsometric measurements using either vacuum deposited gold film on silicon, polycrystalline foil, or the (111) faces of bulk gold crystals. Under potentiodynamic conditions, the cathodic potential vs. current display of a gold electrode shows no hydrogen adsorption from which the real surface area can be determined. However, the real surface area can be estimated from the integrated current contained within the oxygen adsorption

region during the anodic potential sweep or from the oxygen desorption region (22). When compared to the geometric area of the samples, the measured surface areas indicate a surface roughness from 1.3 for evaporated films and 2.4 for polished crystal surfaces. The anodic oxidation of surface disulfide species gives a peak potential that increases positively (for a fixed sweep rate) as the chain length increases. Disulfides are presumed to adsorb primarily as thiolate on gold (111) faces (38). If one assumes that didocosyl disulfide adsorbs as thiolate and converts to sulfonic acid by a five-electron oxidation, it is possible to calculate the original surface coverage from the integrated charge under the oxidation peak and the measured surface area obtained from the total charge contained under the oxygen desorption peak exhibited by the clean gold surface. Such measurements typically yield a coverage between 8 and 10 x 10^{-10} mol/cm^2. The theoretical coverage of a hcp monolayer having 5 Å chain separation is 7.76 x 10^{-10} mol/cm^2.

Film thicknesses were obtained from ellipsometry data of didocosyl disulfide and docosyl thiol and sulfide adsorbed onto freshly evaporated gold foil on polished silicon substrates. These were compared with values obtained from the same compounds adsorbed on electrochemically cleaned polycrystalline and single crystal foils. There is a difficulty in obtaining uniform dielectric constants over the entire surface area of the electrochemically cleaned foils (owing to local variations in surface

roughness). It is, however, possible to obtain meaningful thickness measurements provided one collects the ellipsometry data from the same surface area both before and after adsorption. For didocosyl disulfide the thicknesses so determined were indistinguishable whether the data were obtained from electrochemically cleaned substrates or from the freshly evaporated gold foils. Monolayer thicknesses were within 2-5 Å of the value expected for a fully extended 21 carbon chain (30 Å). Similar results were obtained for docosyl thiol.

Electron diffraction experiments were carried out at 100 kV and 120 kV on a Philips EM 420 transmission electron microscope equipped with a 60-deg eucentric single axis tilting stage. Low-beam current densities at the sample of the order of 2×10^{-5} A/cm^2 were achieved by inserting a 30 μm condenser aperture and by reducing the normal operating filament and emission currents. The area of sample illuminated by the beams was usually 400 μm^2. We did not decrease this area to below 90 μm^2 because of accelerated sample damage. High-speed X-ray film (Kodak Industrex AA-5) was used, allowing a five-fold increase in sensitivity over conventional imaging plates to give satisfactory electron diffraction intensities with a beam dose of between 2×10^{-5} to 4×10^{-5} C/cm^2. Exposures longer than 8-10 sec at this dosage resulted in the irreversible conversion of discrete diffraction spots from the monolayers into continuous amorphous rings. A low-dose unit was employed to prevent radiation damage to areas of the specimen where diffraction information would be

obtained. This unit translated the beam to an unexposed area of the specimen after the camera shutter opened and returned to a preset focusing position after the shutter closed. This translation usually produced a streak on the exposed film whose length depended on beam displacement; the origin of this streak is, however, unambiguous. Because of the progressive degradation of the samples on intermittant exposure, it was not possible to obtain a tilt series within the same sample area; the translation controls were moved slightly before each exposure to produce diffraction from an area previously unexposed to the electron beam. After obtaining diffraction data from any given area of the sample, this same area was usually imaged to be sure it was representative and did not contain any multilayer precipitates. Multilayer precipitates were seen occasionally for the dialkyl sulfide and the dialkyl disulfide.

The thickness of the gold foil could be deduced from subsidiary maxima of extinction contours and was found to range from 400 to 800 Å. The beam orientation with respect to the substrate normal was determined from the underlying identifiable Au reciprocal lattice zones. The precise orientation varied from point to point in the specimen because of the buckling of the gold foils. The radii of curvature of the rumples in the evaporated foils were measured by assigning extinction contours with the goniometer stage tilt axis and sweeping them across a known distance in the image by small tilts determined from the gauge of the sample holder. The range of the curvature radius

was thus found to be 10^6 to 10^7 Å. This elastic rumpling could produce a maximum effective tilt of between 0.01 to 0.1 radians (diameter of selected area over the radius of curvature of the bend) or less than 6^o of tilt. Orientation of the sublattice could be determined by applying the method of Otte, Dash, and Schaack[23] for large camera lengths and that of Laird, Eichen, and Bitler[24] for camera lengths less than 950 mm.

Electron diffraction from single crystal gold foils in (100) and (111) orientations show, in addition to the diffraction spots coinciding with intersections of the reflection sphere and the reciprocal lattice for these orientations, extra spots due to the presence of microtwins and the double diffraction from these structures. A face-centered cubic crystal in (100) orientation is susceptible to twinning on all four (111) planes. This twinning can give rise to additional points in the reciprocal lattice that either coincide with matrix points or are displaced from matrix points by vectors of 1/3 <111>.[25] A selection rule determines whether a twinning plane will produce an allowed twin spot. Conditions for production of these extra spots have been elaborated by Pashley and Stowell.[26] For the case of a beam directed along (100), the diffraction will contain the normal f.c.c. reflections, each at the center of a square array of equidistant satellites displaced from the matrix point by 1/3 <111>.

Normally, (111) films prepared by evaporation onto an epitaxial substrate contain some microtwins. They also contain a

high density of dislocations that pass through the film, giving rise to double-positioning boundaries commonly found parallel to (211) planes. These dislocations can produce extra points belonging to the (111) reciprocal lattice section, but visualization of these require double diffraction conditions to be satisfied.[27]

Stacking faults along (111) planes are commonly found in f.c.c. evaporates. The kinematical theory of diffraction from a random distribution of stacking faults in close-packed lattices has been considered by Paterson,[28] who showed that certain low-angle reflections--particularly {111} and {020} are broadened and displaced along the directions of the stacking faults [111].

In the following, we will need to distinguish between reciprocal lattice vectors of the substrate and of the organic film. For clarity, those vectors pertaining to the substrate will have the designation $[hkl]_S$ and those pertaining to the plane of the monolayer $[uv]_O$.

Results

Docosyl thiol on Au(111). With the electron beam parallel to the $[\bar{1}11]_S$ zone axis of gold, the diffraction from docosyl thiol adsorbed on the $Au(111)_S$ face presents a hexagonally symmetric array of spots with the principal reciprocal lattice vectors coinciding with the $(110)_S$, $(101)_S$, and $(011)_S$ directions in the substrate (Figure 1). The observed spacing of $a^* = 0.2326$ $Å^{-1}$ implies an interchain spacing of $a = (a^* \sin \gamma^*)^{-1} = 4.97$ Å,

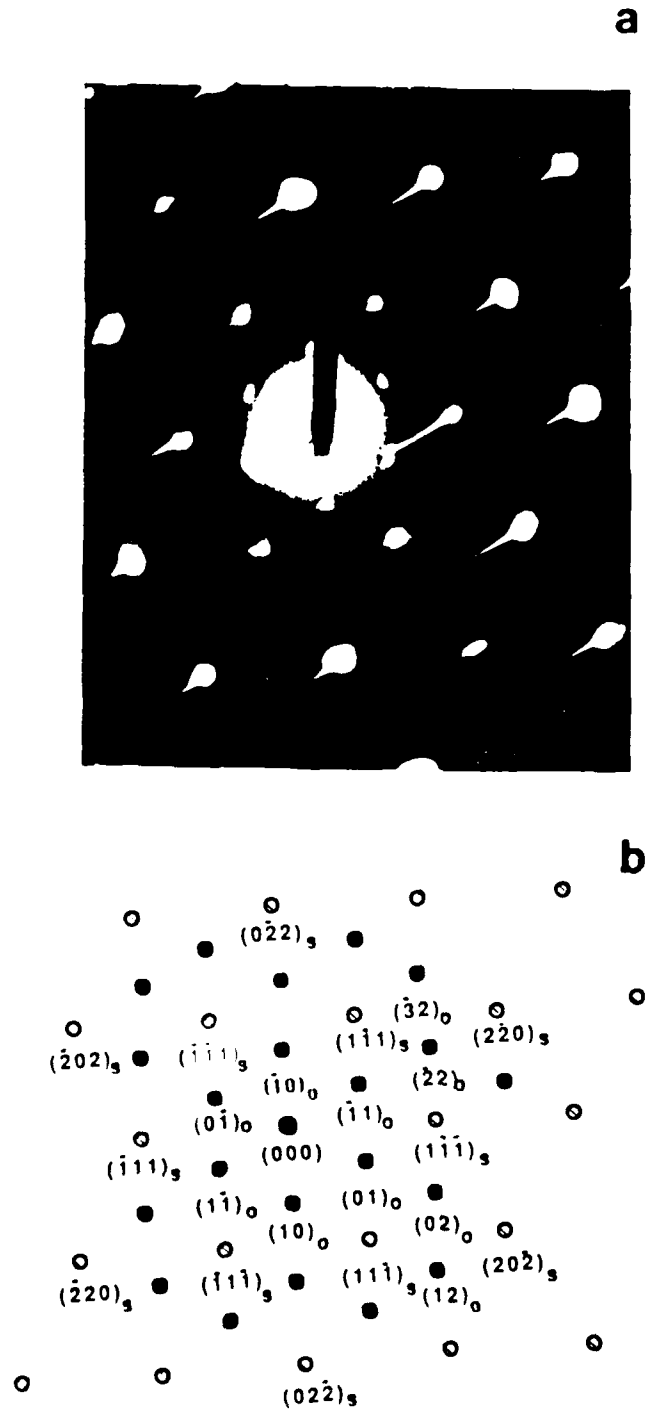

Figure 1. a) Typical diffraction from docosyl thiol on Au(111) with B = $[\bar{1}11]_S$, λ = 0.0335 Å, camera length 1372 mm.
b) Indexing of diffraction spots.

($\gamma^* = 120°$), which is consistent with the model of a freely rotating alkyl chain occupying an area of 21.4 $Å^2$/chain. This spacing is the same found for stearic acid adsorbed on the $(111)_s$ face of silver[1] and is equivalent to the spacing between the next nearest gold atoms on the $(111)_s$ surface (4.99 Å). Although the chain spacings are equal to the second nearest neighbor gold spacings ($\sqrt{3}$), the monolayer lattice vectors lie in the same direction as the principal gold lattice directions (110)s. Thus the monolayer lattice is not strictly epitaxial to that of the gold lattice. The diffraction data are consistent with the coincidence lattice structure[29] represented by the centered lattice c(7 x 7) shown in Figure 2. The error of measurement of interchain spacings ($\pm$0.05 Å) redounds to an uncertainty of $\pm$0.35 Å in the size of this coincidence unit cell.

Diffraction from a similarly adsorbed cyclohexyl mercaptan showed only the expected amorphous scattering, thus demonstrating the dependence of the resulting pattern upon the specific structure of the adsorbate.

Identification of the substrate reflections in Figure 1b reveals weaker $(111)_s$ type spots not normally seen in a [111] section. They are visible in this gold orientation because of the superposition of the first-order Laue zone reflections along with zero-order Laue zone reflections along the $[\bar{1}11]$ zone. The width of the Laue zones depends upon the extension of the reciprocal lattice along the beam direction. For relatively

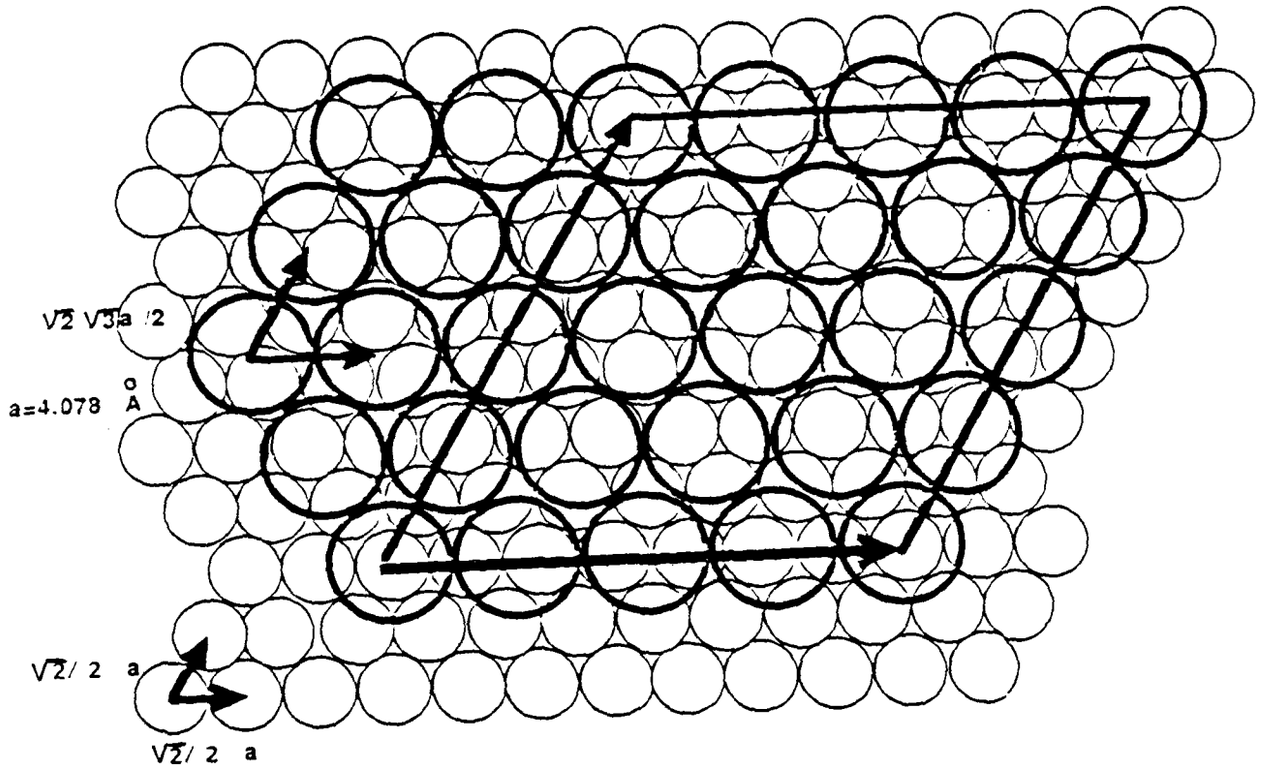

C(7x7)

Figure 2. a) A possible representation of the c(7 x 7) overlayer in which thiol or thiolate groups coordinate with a variable number of gold atoms.

thick crystals, it is quite common for the widths of the zones to overlap.[30]

The $\{11\}_o$ reflections and multiple order $\{10\}_o$ reflections from the monolayer are not easily differentiated from superlattice spots because they overlap with them. In hexagonally symmetric packing, the primary $\{11\}_o$ reflections normally exhibit less than 10% of the intensity of primary $\{10\}_o$ reflections.[31] In order to provide intensity data suitable for structure factor analysis by Fourier methods, one could attempt to correct the observed intensities to account for secondary scattering.[32] Our present interest required only that we approximate the contribution of the superlattice intensities to overlapping zero order $\{10\}_o$ intensities. We make this correction by simple substraction of an adjacent secondary reflection from the primary spot of interest. A radial photometric scan across any of the $(10)_o$ reflections (Figure 3, a and b) reveals a Gaussian intensity distribution with half width at half maximum of 0.0167 $Å^{-1}$. This shape suggests a domain size of 60 Å, about three times the dimension of the coincidence unit cell but significantly smaller than the separation between incoherent twin boundaries in the substrate (~500 Å). A rotational scan through the $(10)_o$ reflections (Figure 3c) shows that the chain packing preserves bond order to within 6°-7° of arc. It is remarkable that there is no evidence of misregistration of the monolayer on opposite sides of the substrate as would occur in the presence of stacking faults.

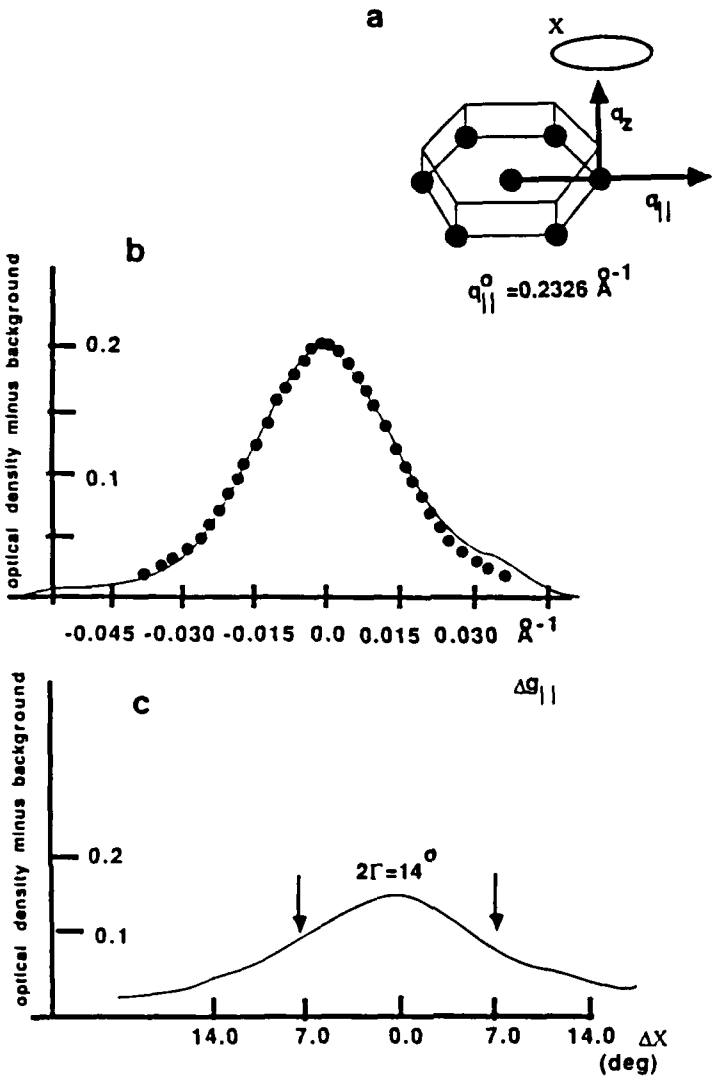

Figure 3. a) The definition of radial ($q_{||}$) and rotational (X) scans through a hexagonal reciprocal lattice. b) A radial photometric scan across a representative $(10)_o$ Bragg spot. Intensity units are arbitrarily based on an optical density scale. Filled circles represent best fit Gaussian line shape of half width 0.0167 Å^{-1}. c) A rotational photometric scan across a representative $(10)_o$ Bragg spot.

Spikes in the reciprocal lattice arising from the form factor for the unit cell allow the same hexagonal $\{10\}_o$ reflections to appear over a broad range of orientations of the beam. With the beam oriented along the $[\bar{1}11]_s$ zone axis, the organic reflections have six-fold rotational symmetry and uniform spot intensity. Since the intensity distribution is determined by the spatially averaged orientations over two sample surfaces, and since this achieves a maximum along the $[\bar{1}11]_s$ zone axis, the average chain orientation must be along the $[\bar{1}11]_s$ direction. (We note that since the two substrate surfaces are antiparallel, there may be some tendency to symmetrize the azimuthal distribution if the chains themselves are approximately parallel (see below, Figure 14).)

The organic lattice spacing and interplanar angles corresponding to $\{10\}_o$ reflections appear to change with orientation depending upon where the reciprocal lattice spikes intercept the reflection sphere.[25] When the electron beam is tilted off the $[\bar{1}11]_s$ zone axis, the six-fold symmetric Bragg reflections seen in orthogonal projections distort to lower symmetry (Figure 4a, b, c). The distortion increases with the magnitude of the tilt angle and is maximal along directions perpendicular to the beam tilt axis. The direction of displacement of reflections of a cubic crystal have been calculated for the general case where the electron beam and the reciprocal lattice spikes pass along different arbitrary directions of the reciprocal lattice.[25] The directions of displacement have been calculated for each of the

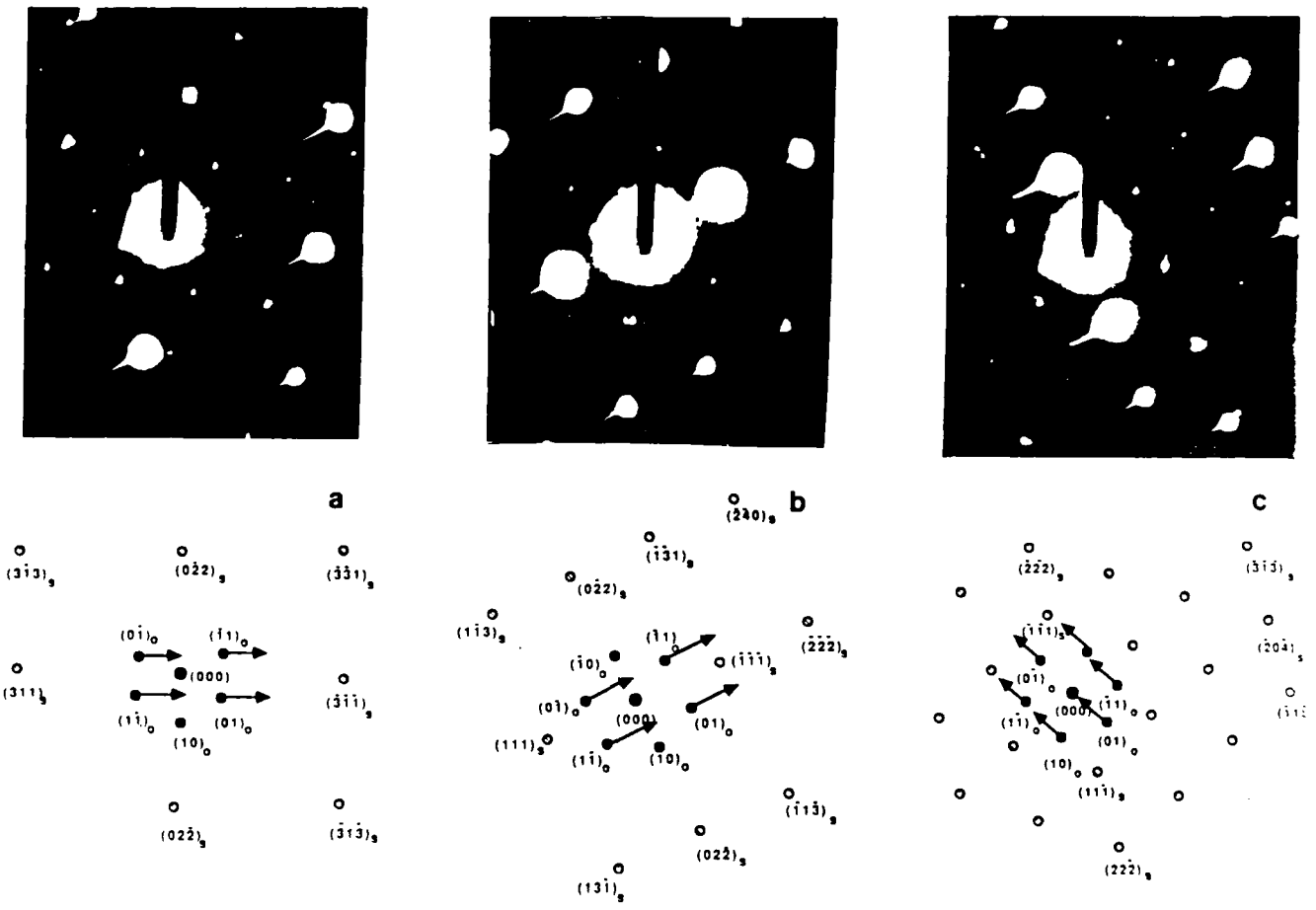

Figure 4. A typical representation of the changes in the thiol diffraction intensity and symmetry with beam tilting. The angle between the $[\bar{1}11]_S$ and beam directions is given below: The direction of the displacements of the organic reflections is given by the arrow. λ = 0.0335 Å. a) B = $[\bar{2}33]_S$, rotation 10°, camera length 1201 mm. b) B = $[\bar{2}11]_S$, rotation 19.5°. camera length 1396 mm. c) B = $[\bar{2}31]_S$, rotation 22.2°, camera length 1189 mm; displacement is along $[\bar{1}\bar{2}4]_S$.

beam orientations shown in Figure 4, assuming that the Bragg rods are on average parallel to the $[\bar{1}11]_S$ zone axis, i.e., they have no preferred azimuthal direction. The calculated splitting directions are in agreement with the data, thus reinforcing the conclusion drawn from the uniform and symmetric spot patterns.

Garoff et al.[33] have shown that it is possible to evaluate the spatial average inclination of paraffin chains from measurement of the intensity falloff of the $\{10\}_O$ reflections with increasing beam tilt. In the kinematic limit, scans of the diffracted intensity along the Bragg rods normal to the substrate have roughly a width inversely proportional to the thickness of the monolayer. The thickness decreases for increasing angle of chain tilt. In the present example, however, several complications arise. A complete tilt series from one area of the specimen cannot be obtained owing to sample lability in the beam. Further, the tilt angle changes from place to place on the sample owing to buckling of the gold foil. The simultaneous diffraction from the substrate as well as from the organic film, however, allows determination of the beam orientation for any given exposure. The identification of the zone axis from an observed combination of Bragg reflections of the substrate orients the beam with respect to the substrate. A factor less readily overcome in measuring fall-off in intensity with beam tilt is the variable substrate attentuation resulting from the dynamical scattering from the gold substrate. Extinction distances for all low-order gold reflections are below 300 Å[33]--substantially less

than the substrate thickness. Therefore, transmitted and diffracted beam intensities from the organic film will be reduced by systematic multiple reflections from gold. The magnitude of this reduction depends in a complicated way upon the particular reciprocal lattice points intercepted, their extinction distances, the deviation parameter, and the specimen thickness.

Diffraction data were obtained from discrete beam orientations, including the following sets of zone axes: $[\bar{1}11]_S$, $[\bar{2}11]_S$, $[\bar{2}31]_S$, $[\bar{2}21]_S$, and $[\bar{2}33]_S$. This series constitutes up to 23° of tilt with respect to $[111]_S$. Figures 4a, b, and c show the general intensity of the $(10)_O$ reflections with increasing tilt angle. To circumvent the problem of anomalous absorption producing false monolayer spot intensities, the sample was rotated around a common rotation axis ($[0\bar{1}1]_S$ for (111)Au, see Figures 4a, b) and the intensities of all first-order monolayer reflections were measured. The reflections parallel to the rotation axis have an effective $q_z = 0$ component, while those off axis have the q_z component given by the deviation parameter $q_z = q_{||}{}^{O} \tan \theta$, where θ is the rotation angle. The intensities of these off-axis reflections were divided by the intensities of the on-axis reflections after subtracting the contributions of overlapping superlattice monolayer reflections. We plotted the peak intensities so obtained versus the corresponding q_z value for the $[\bar{2}33]_O$ and $[\bar{2}11]_S$ beam orientations (Figure 5). Although there is measured noise in the resulting normalized intensity data, it is clear that the sample exhibits Bragg spikes out

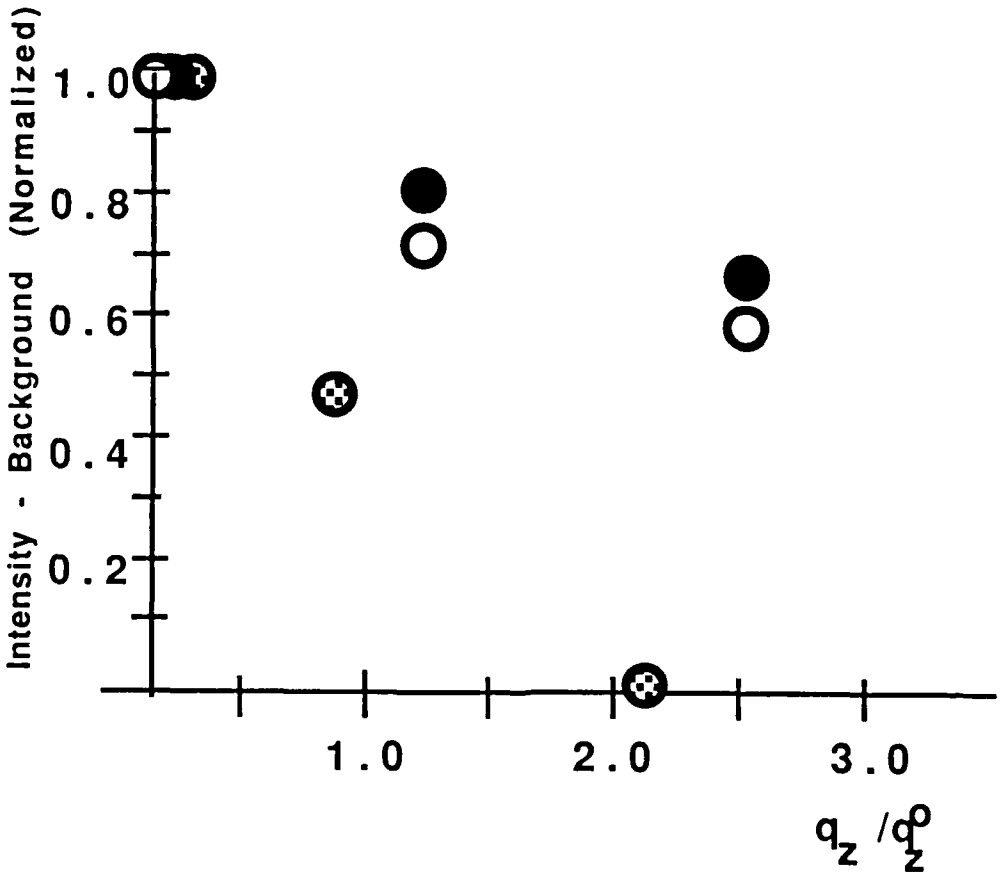

Figure 5. The variation of photometric intensity of monolayer reflections with q_z at X = 0 and constant $q_{||}$ for Au(111) and Au(100). $q_z^o = 2\pi/\text{length of hydrocarbon chain}$ (1.04 Å + 1.8 Å + 21/2 x 2.54 Å) = 0.213 $Å^{-1}$. Filled circles: $(10)_o$ reflections from didocosyl disulfide on $(111)_s$, $q_{||}^o = 1.4615$ $Å^{-1}$. Open circles: $(10)_o$ reflections from docosyl thiol on $(111)_s$, $q_{||}^o = 1.4615$ $Å^{-1}$. Checkered circles: $(11)_o$ reflections from didocosyl disulfide on $(100)_s$, $q_{||}^o = 1.3840$ $Å^{-1}$.

beyond q_z = 0.5 $Å^{-1}$ corresponding to θ = 20°. At half intensity, q_z is estimated to be between 0.6 to 1.0 $Å^{-1}$, corresponding to θ = 25°-35°.

Docosyl thiol on Au(100). Docosyl thiol adsorbed on the (100) face of gold exhibits diffraction spots on a square array oriented along the gold lattice vectors $[100]_S$ and $[010]_S$ (Figure 6a). The spacing along these directions is equivalent to 0.2203 $Å^{-1}$ and corresponds to an interchain spacing of 4.54 Å. The square array is similar to that seen in a (001) section of the reciprocal lattice for a base-centered square lattice. The four observed reflections would lie along the $[11]_O$ and $[\bar{1}1]_O$ directions, rotated by 45° with respect to the substrate $[110]_S$ and $[\bar{1}10]_S$ directions (Figure 6b). Apparently, the expected $(20)_O$ reflections, if present, are too weak to be detected, or are completely suppressed by disorder in the organic lattice. The $(10)_O$ reflections are forbidden by the structure factor for a base-centered cell. The absence of $(20)_O$ and high-angle reflections make this identification subject to the theoretical evaluation of the structure factor under conditions of imperfect translational order. We have not yet undertaken this calculation to see what kinds of disorder produce the measured intensities. The most likely assumption is that tilt variations or screw displacements along the chain axis suppress the high-order reflections.

The two-dimensional unit cell for such a base-centered structure is a square 6.42 Å on a side with corner and base-

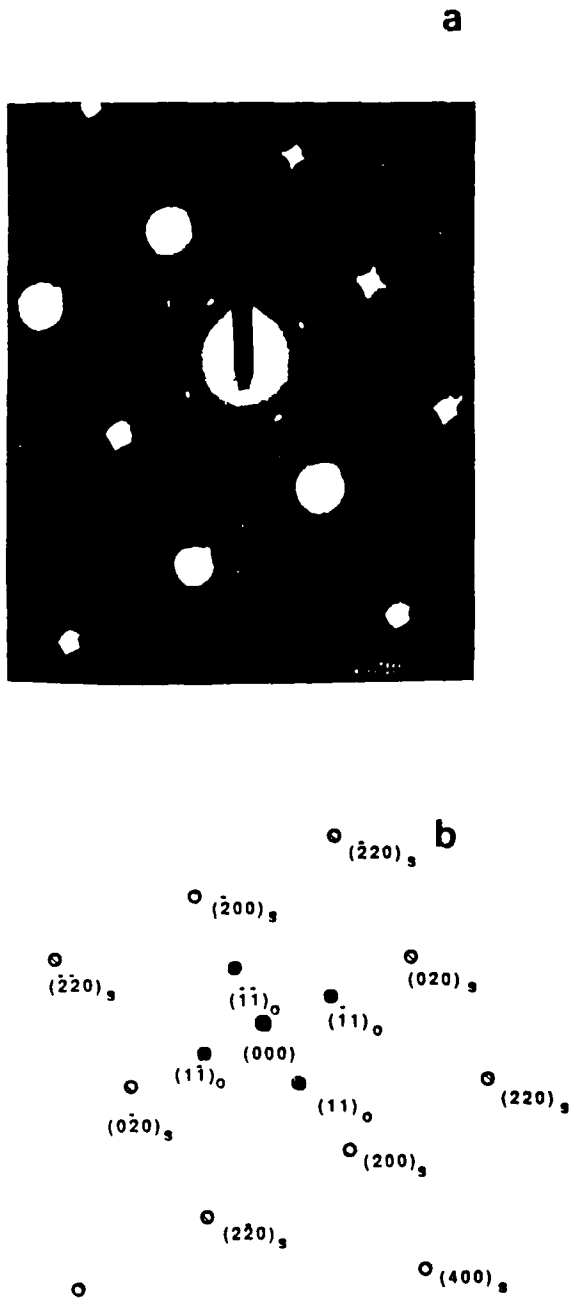

Figure 6. a) Typical diffraction from docosyl thiol on Au(100), cameral length 1467 mm, λ = 0.0335 Å, B = $[001]_S$. b) Indexing of observed reflections.

centered paraffin chains. The packing density is 20.6 $Å^2$ per chain. The chains have a spacing that does not conform to the free rotator model; presumably neighboring chains are locked into stationary positions determined by the overlapping van der Waals' lobes of the methylene groups (see Figure 7).

No other primary organic reflections are visible. Separate superlattice satellites are seen around each gold $[001]_S$ zone reflection. Unlike the case of adsorption in the $(111)_S$ face, the monolayer spacing seems to be incommensurate with the gold spacings. Since the spacing is a rational multiple (10/9) of the <100> lattice spacing and the reflections are parallel to the gold lattice edge vectors we identify the overlayer as deriving from the coincidence overlayer: c(10 x 10) (Figure 7). The absence of all reflections for a base-centered square lattice other than those for which $(h,k)_O = (\pm1,\pm1)$ may mean that for translation to corresponding points from one chain to the next across the substrate, the displacements become more variable the longer the surface translations. This would have the effect of randomizing the phase relationships for equivalent points on neighboring chains. If the structure were under the control of multiple coordination sites, small tilt or translational displacements of chains would be likely and would have the same effect.

Translational order is appraised by obtaining a radial photometric scan of the intensity through the $(11)_O$ diffraction plans. The data appear to fit a Lorentzian distribution. A

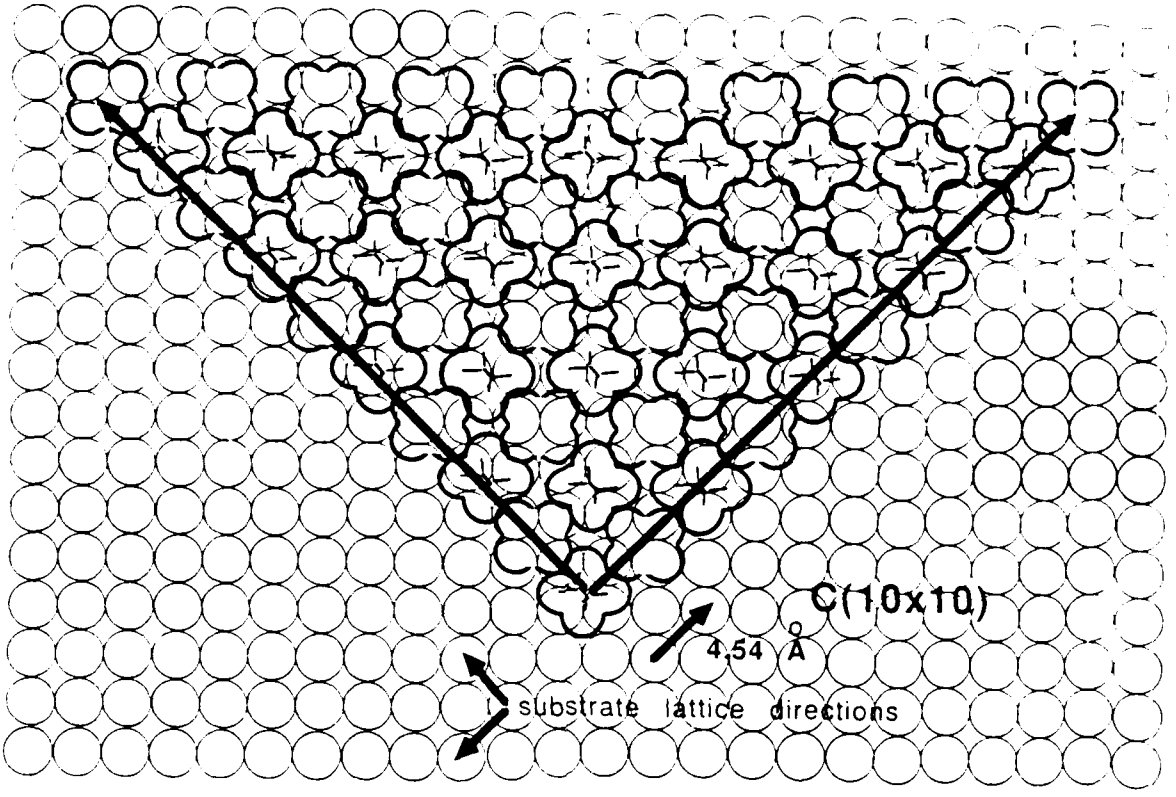

Figure 7. A possible representation of the coincidence c(10 x 10) overlayer on the Au(100) face. Only half of the centered lattice is drawn. Planes of the zigzag chains are not to be inferred from this illustration.

measured half-width at half maximum intensity (HWHM) of 0.0075-0.005 $Å^{-1}$ (Figure 8a, b) corresponds to a correlation length of 130-200 Å. This length is somewhat shorter than the spatial frequency of microtwins in the gold foil; it approximates, however, the distance spanned by 3 to 4 coincidence lattices placed side by side. The angular distribution of intensities along the X direction in Figure 8c has an HWHM of 5°-6° indicating strong (head group) bond-directed order conforming to the orientation of the substrate.

Didocosyl disulfide on Au(111). The diffraction from didocosyl disulfide (RSSR) on Au(111) presents no outstanding differences from docosyl thiol on Au(111). Interchain spacings (4.97 Å), domain size (60 Å), and bond directed ordering (hexagonal array with an angular spread of 12° (FWHM) centered about the gold hexagonal lattice) are indistinguishable from the thiol. Measurements of the disulfide spacings also show hexagonal symmetry for the case of zero beam tilt (beam parallel to $[\bar{1}11]_S$). This symmetry, together with the uniform intensity of these spots, indicates that the zigzag chains have no preferred azimuthal direction. At the same time, the intensity of the $\{10\}_O$ reflections also appears to fall slightly less rapidly with increasing q_z than the fall-off for the corresponding thiol (see Figure 5), although the error of measurement does not enable accurate quantification of these differences. Figure 9a, b, c shows a series of diffraction photographs in which the beam tilts from the $[\bar{1}11]_S$ to the $[\bar{2}31]_S$ zone axes. The average chain tilt

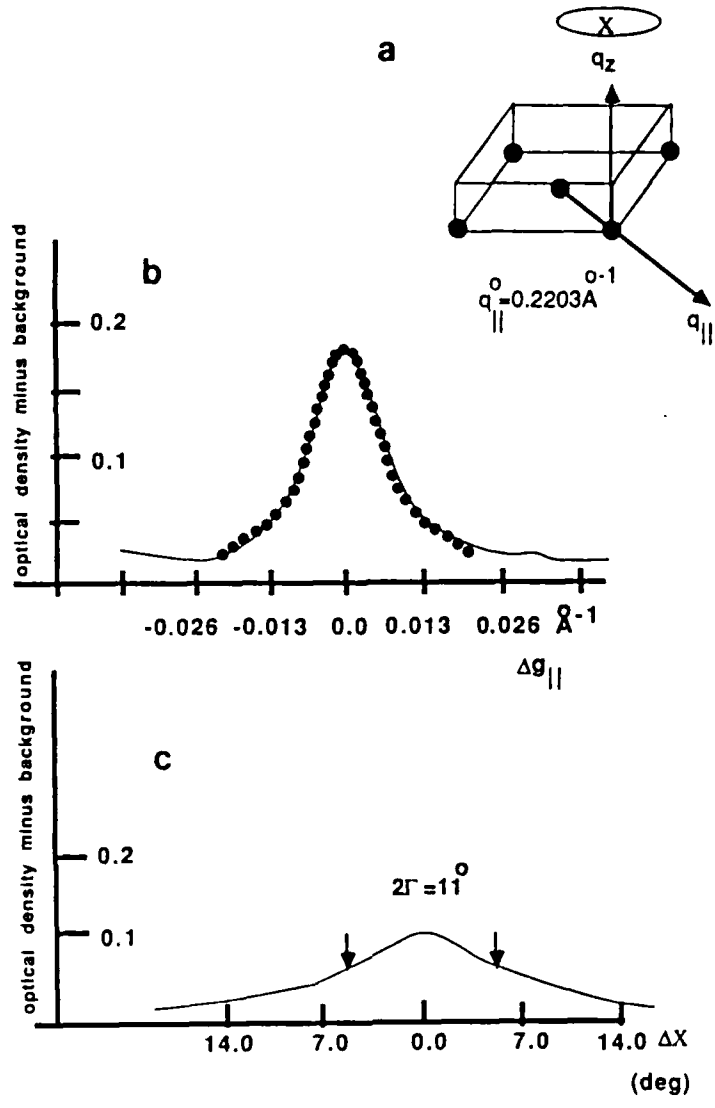

Figure 8. a) Definition of a radial ($q_{||}$) and rotational (X) scan through the reciprocal lattice of a base-centered rhombohedron reciprocal lattice. b) A radial photometric scan through a $(11)_o$ Bragg spot. Intensity units are arbitrarily based on an optical density scale. Filled circles represent best fit Lorentzian line shape of half width 0.00468 $Å^{-1}$. c) A rotational photometric scan across a representative $(11)_o$ Bragg spot.

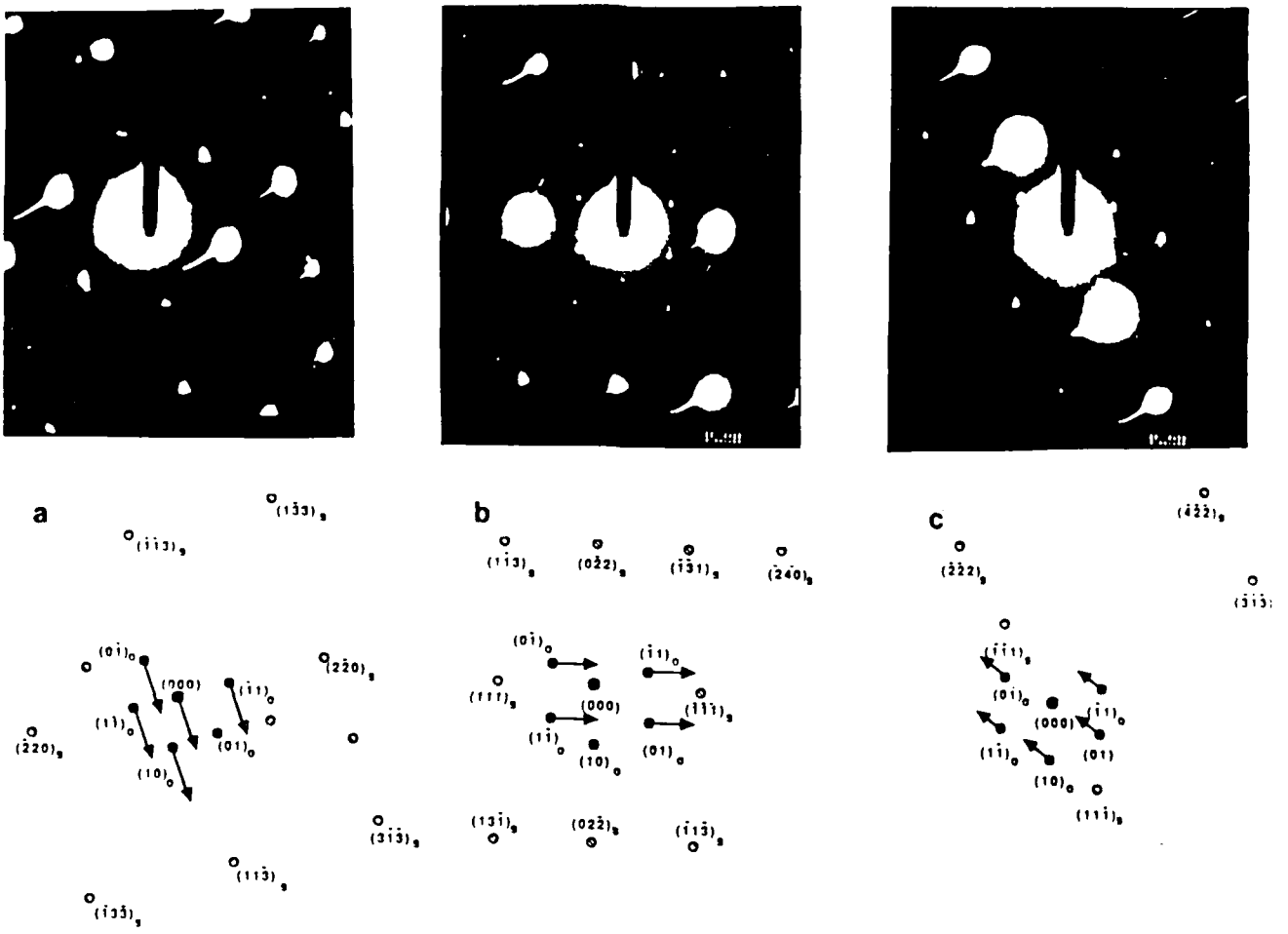

Figure 9. Typical diffraction from didocosyl disulfide on Au(111). Direction of splitting of organic reflections shown by arrow. λ = 0.0335 Å. a) B = $[332]_S$, camera length = 1375 mm. b) B = $[\bar{2}11]_S$, camera length = 1452 mm. c) B = $[\bar{2}31]_S$, camera length = 1467 mm. Spot displacement along $[\bar{1}\bar{2}4]$.

appears to be at least as great as that of the corresponding thiol. Like the thiol, the symmetry and uniform intensity of the $(11)_o$ reflections for zero beam tilt suggest that the paraffin chains have a tilt direction that is symmetrized about the substrate normal.

In preparing didocosyl disulfide monolayers, we discovered that if we allowed excessively long intervals of adsorption (a period exceeding 24 h), multilamellar crystalline structures formed. These have the appearance of quasi regular patterns of closely spaced spots (speckling) that appear to be centered about a heavier primary spot (Figure 10). This effect has been observed in a pattern from polycrystalline diacetyl by Cowley et al.[32] and has been attributed to secondary diffraction from layers of crystal varying by a few degrees in orientation. It is an example of the rotational slip between crystalline layers leading to polycrystalline domains. In this case long adsorption periods occasioned the formation of multiple layers with no registry between layers.

Didocosyl disulfide on Au(100). Like the corresponding thiol, didocosyl disulfide on Au(100) presents diffraction spots in a square array of uniformly intense spots directly along the $[100]_s$ and $[010]_s$ axes. The spacing is 0.2203 $Å^{-1}$ (4.54 Å) (Figure 11a, b). As previously explained, these spots were attributed to the $(11)_o$ and $(\bar{1}1)_o$ reflections of a base-centered square lattice. Higher order $(hk)_o$ reflections were not observed. A translational correlation length of ~130 Å-200 Å was

Figure 10. Example of multiple diffraction through a multiple layer of didocosyl disulfide in which a stacking disorder leads to the observed speckling pattern. Camera length = 1348 mm, λ = 0.0335 Å.

measured. Measurement of the decrease of intensity of the $(11)_o$ reflections as the beam is rotated about the $(100)_s$ axis indicates that total extinction occurs for a rotation of less than 18° (see Figure 5). This was determined by tilting the beam to coincide with the $[013]_s$ zone axis. An accurate measurement of the average chain tilt is not yet possible owing to the limited amount of data collected, yet it is clear that it is significantly less than the tilt exhibited on (111)Au. We estimate the average tilt angle to be between 6-12°.

Unlike the case of docosyl thiol, however, exceptionally sharp and rather weak reflections are also seen along the $[110]_s$ and $[\bar{1}10]_s$ directions (Figure 11a, b) and, less commonly, along $[100]_s$ and $[010]_s$ (Figure 11c). These reflections have a spacing between 0.196-0.198 $Å^{-1}$ (5.10-5.05 Å). Up to three orders of reflections are observed. The absence of a complete array of $(10)_o$ reflections again suggests a base-centered square lattice. Here, the dimensions are about 7.14 Å on a side, yielding a more loosely packed structure with a density of about 25.5 $Å^2$/chain. The chain spacings suggest freedom of methylene group rotation. When the edges of the unit cell are oriented along $[100]_s$ and $[010]_s$ (i.e. $[10]_o$ is parallel to $[100]_s$ and $[01]_o$ parallel to $[010]_s$, Figure 12a), the spacing in the $[11]_o$ and $[\bar{1}1]_o$ directions is incommensurate with the gold spacings (actually 7/8 $\sqrt{2}$ a), and the overlayer corresponds (Figure 12a) to a coincidence lattice of the type c(7/2 $\sqrt{2}$ x 7/2 $\sqrt{2}$). When the edges of the unit cell are oriented along $[110]_s$ and $[\bar{1}10]_s$ (i.e.

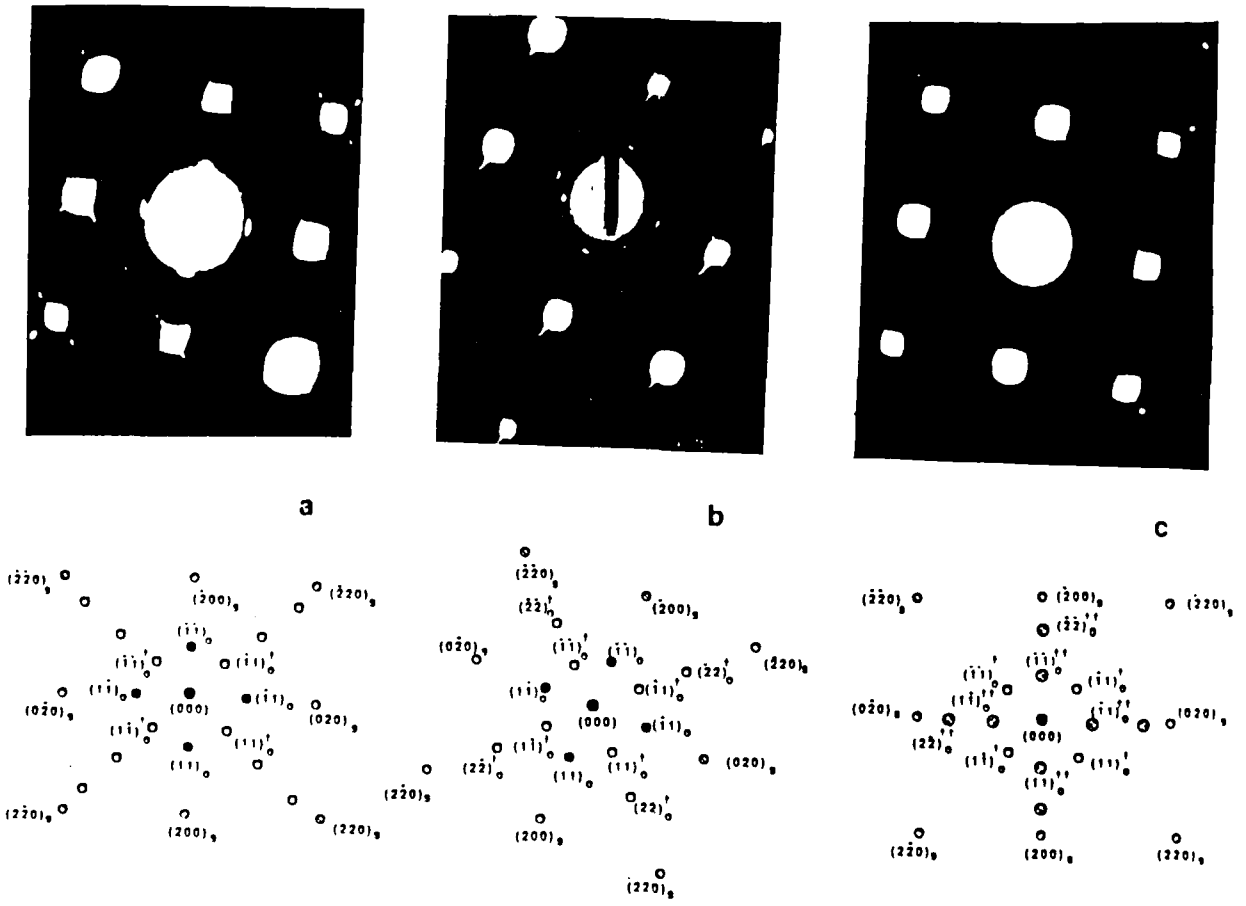

Figure 11. Typical diffraction patterns from didocosyl disulfide exhibiting three different phases of packing on Au(100), B ≅ $[001]_S$, λ = 0.0370 Å. Lower: Indexing the reflections of three different base-centered rhombohedra: The c(7/8 √2 x 7/8 √2) overlayer reflections are identified by $(hk)_o^+$; the c(5/4 x 5/4) overlayer reflections are identified by $(uv)_o^{++}$.
a) Monolayer reflections exhibiting predominately the c(10 x 10) overlayer, camera length = 1463 mm.
b) Monolayer reflections exhibiting both the c(10 x 10) and the c(7/2 √2 x 7/2 √2) overlayers, camera length = 1499 mm. c) Monolayer reflections exhibiting the c(7/2 √2 x 7/2 √2) and c(5 x 5) overlayers, camera length = 1502 mm.

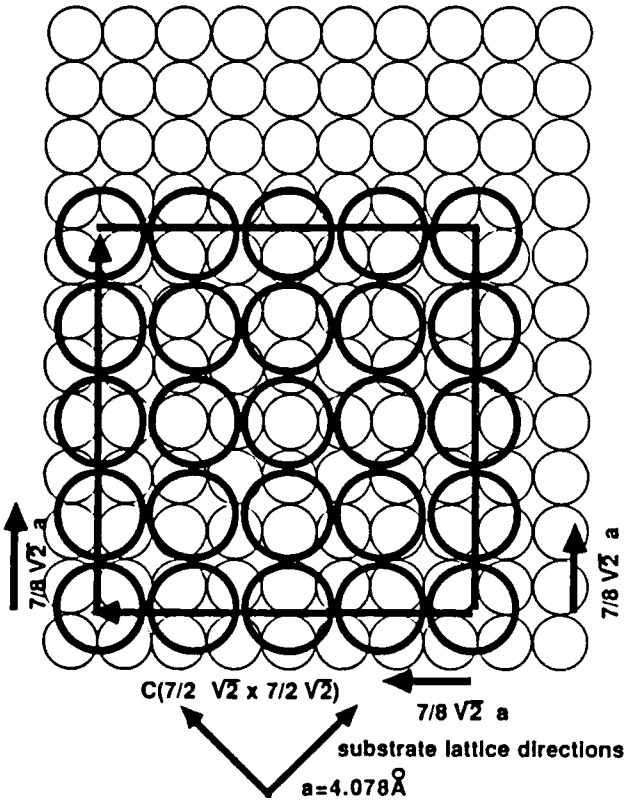

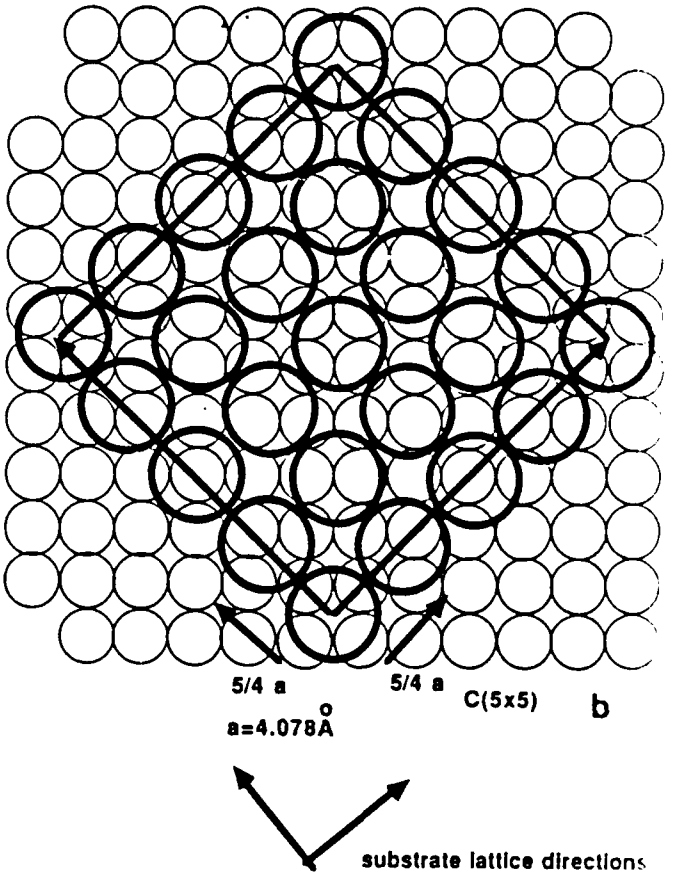

Figure 12. a) A possible representation of the c(7/2 √2 x 7/2 √2) overlayer of didocosyl disulfide on Au(100). Each sulfide group alkyl is assumed to have rotational symmetry and variable coordination with surface Au atoms. b) A possible representation of the c(5 x 5) overlayer of didocosyl disulfide on Au(100). Each sulfide alkyl group is assumed to have rotational symmetry and variable coordination with surface Au atoms.

$[10]_o$ is parallel to $[110]_s$ and $[01]_o$ is parallel to $[\bar{1}10]_s$ the monolayer unit cell is rotated 45° with respect to the gold sublattice), then the spacing in the $[11]_o$ and $[\bar{1}1]_o$ directions is also incommensurate with the gold spacings (actually 5/4 a), and the overlayer corresponds (Figure 12b) to a centered lattice of the type c(5 x 5). Neither $(20)_o$ nor any higher angle reflections are detected.

Photometric scans in the rotation direction (X) show an equivalent magnitude of bond disorder for all monolayer phases. The angular spread of $(11)_o$ and $(\bar{1}1)_o$ reflections is 14° (full width at half maximum). Of the lowest density phases, radial scans indicate a translational order better than 0.002-0.003 $Å^{-1}$, which is two times sharper than that seen for the c(10 x 10) square overlayer reflections. Reflections from the c(7/2 $\sqrt{2}$ x 7/2 $\sqrt{2}$ overlayer were used to estimate the outside limits of instrumental broadening to all measured line widths. Line widths of these reflections corresponded, roughly, to the spatial frequency of substrate imperfections ((111) microtwins on a (100) surface have an average separation of 400-500 Å).

Beam tilting measurements indicate that while both the high density and low density square overlayers have conformations in which the average chain tilt exhibits rotational symmetry with respect to the substrate normal, the low density square reflections quench much more rapidly with variation of q_z than do the high density reflections. Their intensity falls below visibility for q_z = 0.1 $Å^{-1}$, indicating that on average the

paraffin chains in the low density square phase are tilted very slightly, if at all (<6°).

Didocosyl sulfide. Multilayer precipitates of didocosyl sulfide grown overnight from ethanol on Au(100) present an orthorhombic crystalline lattice (Figure 13a, b) with cell dimensions a = 7.71 Å and b = 5.0 Å. Monolayer films, however, assembled in appreciably shorter times (1-2 h) and thoroughly rinsed with solvent exhibit the same basic features as monolayer films of didocosyl disulfide. Monolayer films of didocosyl sulfide assembled on Au(111) also present indistinguishable diffraction results as didocosyl disulfide on Au(111) (Figures 6 and 9). In consideration of the larger difference in binding affinity of sulfide and disulfide for gold,[35] we suspect that trace disulfide impurities might be responsible for the observed diffraction results. More work is needed in quantifying the amount of sulfide bound before we can safely conclude that it has a packing isomorphous with that of the disulfide.

Discussion and Summary

TEM data of self-adsorbed docosyl thiol, and didocosyl disulfide on crystalline Au surfaces show these alkanes to be packed in disordered crystalline (or paracrystalline) arrays, with long-range bond orientational correlations and varying translational correlations (see Table I). Substrate atom symmetry and spacings play an important role in establishing the details of their molecular packing. A hexagonal close-packed

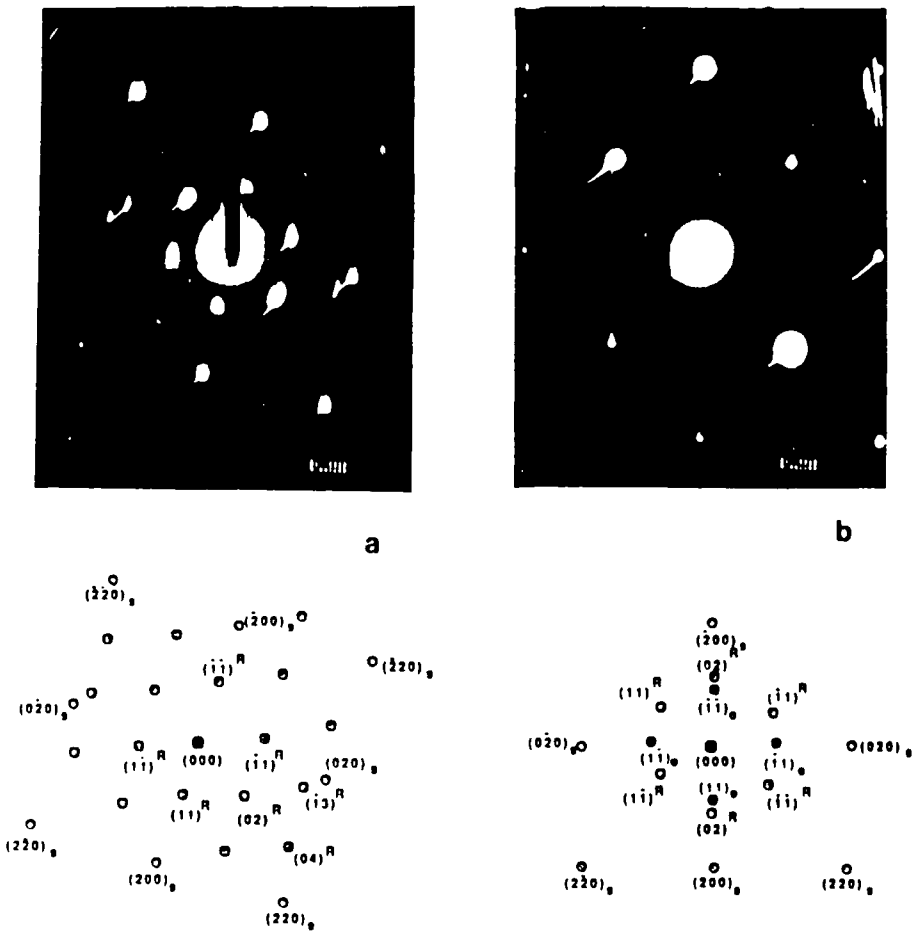

Figure 13. a) An example of the orthorhombic reciprocal lattice obtained from a multilayer precipitate of didocosyl sulfide. Lattice constants are a = 7.71 Å and b = 5.0 Å. Orthorhombic reflections are identified by (hk)R. b) The transition from monolayer to multilayer in which the four-fold symmetric c(10 x 10) overlayer is present along with the orthorhombic multilayer.

Table I. Summary of the Structural Phases for Organosulfur Compounds on Gold

Gold Face	Overlayer Type	Repeating Unit	Two-Dimendional Unit Cell	Unit Cell Length (Å)	Interchain Distance (Å) ± .05 Å	Packing Density Å^2 /chain	Translational Correlation Distance (Å)	Polar Angle of Chain Tilt (θ)
Docosyl Thiol								
(111)	incommensurate	c(7 x 7)	hcp	b = 4.97	4.97	21.4	60	25-35°
(100)	incommensurate	c(10 x 10)	base centered square	a = b = 6.42	4.54	20.6	130-200	--
Didosocyl Disulfide								
(111)	incommensurate	c(7 x 7)	hcp	b = 4.97	4.97	21.4	60	25-35°
(100)	incommensurate	c(10 x 10)	base centered square	a = b = 6.42	4.54	20.6	130-200	6-12°
(100)	incommensurate	c(7/2 √2 x 7/2 √2)	base centered square	a = b = 7.14	5.05	25.5	>300	<6°
(100)	incommensurate	c(5 x 5)	base centered square	a = b = 7.2	5.10	25.9	>300	<6°

(hcp) distribution of surface gold atoms (i.e., a (111) face) gave in-plane diffraction data exhibiting two-dimensional hexagonal space groups with spacings and orientations conforming to the coincidence overlayer c(7 x 7) for all three head groups. The interchain spacings (4.97 Å) are sufficiently long that the intermolecular contacts should permit CH_2 group rotation. Spacings between alkyl chains were slightly larger than the spacings found for hcp-LB films of Cd-stearate,[33] lipid[36] and fatty acid monolayers.[37] Head group bonding is presumed to impart some differences compared to structures in which the end groups are unconstrained. The density of the unit cell is slightly smaller in disulfides and thiol monolayers than in other alkane microcrystals (area per chain is 21.4 $Å^2$ for didocosyl disulfide and docosyl thiol, and 21 $Å^2$ for Cd stearate, compared to 20 $Å^2$ for anhydrous phospholipids and lecithin[31]).

The presence of superlattice reflections overlapping the higher harmonic monolayer Bragg reflections complicates the comparison of experimental intensities with structure factor calculations for ideal lattices, making it difficult to quantitate the degree of crystalline order. The correlation lengths for disulfide and thiol are similar: 60 Å based upon $(10)_o$ reflections, and the line shapes appear to fit a Gaussian function. This is slightly greater than the domain size that Garoff et al.[33] found for the Langmuir-Blodgett monolayer of cadmium stearate, although the line shape in the stearate monolayer fitted a Lorentzian better than a Gaussian function.

The mismatch between the head group separation and preferred tail group separation in similar constrained alkyl systems suggests the possibility of accommodation in sulfide alkyls by chain tilting.[13] In Cd stearate, the spot intensity changed with sample orientation in a way that suggested that the long axes of the stearate molecules were tilted, on average, some 8° away from the surface normal. The tilt direction, however, is disordered. Nuzzo, Fusco, and Allara,[14] and Porter et al.[16] have obtained the infrared reflection absorption spectra of various chain length disulfides and thiols adsorbed on evaporated gold foil having predominately (111) texture. They interpreted the relative strengths of CH stretching modes as resulting from fully extended alkyl chains tilted between 20-30° off the substrate normal. Our beam tilting experiments also indicate a substantial amount of chain tilt in didocosyl disulfide and docosyl thiol. For example, the intensity of the $\{10\}_o$ Bragg spots does not diminish to below half maximum until the sample is tilted at least 25° from the $q_z = 0$ plane. The pattern of spot displacement with various amounts of sample tilting and the symmetric distribution of spot intensity when the beam is parallel to the substrate normal demonstrate that the direction of tilt is averaged over the azimuthal plane in such a way as to produce effective Bragg spikes in the direction of the substrate normal. If there were only a few directions of tilt along discreet gold surface vectors that could satisfy these conditions, it is conceivable that the effect of having a double-sided sample would be to produce a

false averaging of the azimuth (see Figure 14). It is more likely, however, that the tilt direction is uniformly disordered on this surface.

Nuzzo et al.[38] compared X-ray photoemission and electron energy loss data on vapor adsorbed dimethyl disulfide with that of the corresponding thiol and concluded that on the $[111]_S$ face of gold single crystal the chemisorption occurs predominately dissociatively as thiolate (RS), although a smaller component is believed to adsorb molecularly. This may explain the lack of any discernable difference in the diffraction on Au(111) from didocosyl disulfide and docosyl thiol. The absence of any further distinguishing characteristics in diffraction from didocosyl sulfide is interpreted as originating from either similar chain packing, despite the single bridging sulfur, or to the presence of impurity disulfides whose binding affinity to the gold surface is orders of magnitude greater than the sulfide. Beam tilting experiments are presently too incomplete to differentiate the effects of head group substitution on the canting of the molecular axis in these cases.

On the (100) face, a square array of substrate atoms produces two dimensional square alkane lattices. Three different disordered crystalline phases are observed for the didocosyl disulfide (RSSR); only a single phase is observed for docosyl thiol (RSH) (see Table I). In all phases, the systematic absence of reflections, other than those satisfying the condition

$$h + k = 2n \qquad (n = 0, 1, 2, \text{etc.})$$

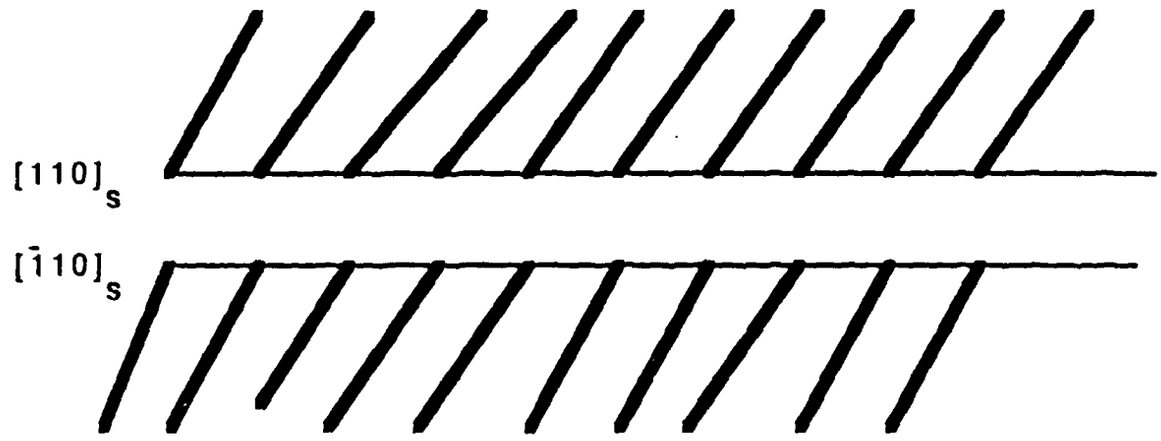

Figure 14. A representation of the way in which the double sided sample might falsely symmetrize the tilt direction of alkyl chains.

indicate base-centering of the two-dimensional square lattices. The phase common to all head groups exhibits an interchain spacing of 4.54 Å, which is short enough that intermolecular contacts will determine the azimuthal orientation of each chain (see Figure 7). The spacing is a rational multiple (10/9) of the gold lattice spacing. The overlayer is therefore presumed to be the coincidence centered lattice c(10 x 10). Either variable substrate coordination symmetry (three to four coordinating Au atoms) or point defects in the chain (trans-gauche replacement) is expected to produce this packing.

In this phase, only the four reflections (h, k) = ($\pm$1, $\pm$1) are observed. The missing (2n, 0) and higher harmonic (h, k) reflections are presumed to be smeared out either by small lattice deformations or Debye-Waller fluctuations. In both cases, the reflections would become more and more diffuse in all directions with increasing distance from the central reflection. Packing could be more variable for this phase because azimuthal alignment of adjacent chains would be coupled both to substrate roughness and to chain tilt.

Despite the absence of a simple, common lattice match with gold, the c(10 x 10) square phase shows crystalline order over 130 Å-200 Å in the direction parallel the nearest neighbor vectors. Evidently ordering in the $\{11\}_o$ directions is benefitted by nearest neighbor contacts. Positional correlation in the $\{10\}_o$ directions (direction of the gold face diagonals) could be considerably less. The statistics describing the

fluctuations of the unit cell edge need not be the same as those describing fluctuations of the shortest intermolecular vector. Despite this evidence of poor translational ordering in one direction, the alkyl chains retain Au-S substrate bond directed order to within $\pm 6^{\circ}$ over the entire area intercepted by the probe (400 μm^2). Given the presumed variability of Au-S coordination for this phase, such bond directed ordering is remarkable. It is probably reinforced by strongly directed interchain contacts (see Figure 7).

Didocosyl disulfide forms several different incommensurate phases on Au(100), whereas docosyl thiol appears to form only one. One possible explanation of these differences derives from the observation by Nuzzo, Zegarski and Dubois[38] that, although the dominant, stable chemisorbed state of dimethyl disulfide on Au(111) is as a thiolate, some strongly chemisorbed disulfide is retained, and there may be an equilibrium between the disulfide and the thiolate on the surface. There is the possibility that both disulfide and thiolate phases exist on an Au(100) surface. We expect the disulfide chains will pack less densely than the corresponding thiolate chains, because the presence of the disulfide bond limits the conformations available for intramolecular chain packing and may preclude the interchain registration that allows short intermolecular contacts (4.54 Å). We suspect that the phases observed to have long spacings (5.1 Å) may be attributable to surface disulfides and the phase observed to have short spacings (4.54 Å) may be attributable to surface

thiolates. Thiolates may be able to exist in either phase, but steric requirements may limit disulfides to the phase with the longer chain spacings. The single phase observed on Au(111) for didocosyl disulfide may actually be two phases, but the disulfide phase may be masked by its ability to pack into hcp lattices having longer chain spacings (5.0 Å).

The question whether the disorder in these monolayer systems is liquid-like or microcrystalline revolves around whether translational correlations decay exponentially with distance or are truncated by a series of defects that preserve bond order. Liquid-like phases could resemble the hexatic (for hexagonal lattices) or tetratic (for square lattices) states of liquid crystals.[39] Unfortunately, the present data do not yield sufficiently accurate statistics on the tilt and positional disorder in these systems to provide unequivocal answers.

The nearest neighbor spacings of the c(10 x 10) phase (4.54 Å) are similar to those found in paraffin crystals with orthorhombic unit cells having rectangular sublayers (4.5 Å), i.e., those in which the chain axes are orthogonal to the plane of the end groups (designated R[0,0] in Kitiagorodskii's notation[6]). In these bulk paraffin crystals, the CH_2 groups in adjacent chains are coplanar, and the chains themselves are untilted. The two-dimensional monolayers have a unit square cell 6.42 Å on a side (surface area per chain 20.6 $Å^2$) compared to the bulk paraffin orthorhombic R[0,0] structure with rectangular two-dimensional cell (5.0 x 7.42 Å) (18.6 $Å^2$ per chain). The reduced

packing density of the disulfide and thiol monolayers compared to that in the terminally unconstrained case again leads one to suspect that there may be substantial canting of the molecular axes in the direction of maximum monolayer void volume, i.e., in the direction of the gold unit cell surface diagonal vectors $\{110\}_S$. One may speculate that it is a variation in the angle of tilt along these directions that is in part responsible for the absence of the $\{20\}_O$ and high order reflections in this system.

Some evidence exists to indicate that chain tilt of the square lattice may be less than that encountered in the hcp lattice. One measurement of a $\{11\}_O$ reflection from docosyl disulfide at a $q_z = 0.463$ (beam orientation 18.5° away from the substrate normal) showed no residual intensity remaining, while the intensity of a spot from the hcp phase at a roughly equal q_z value measured about 0.6-0.7 times the maximum value obtained at $q_z = 0$. Thus, the polar tilt of this square overlayer may be considerably less than that in the hcp phase. The direction of the spot distention on beam tilting is consistent with an average orientation of reciprocal lattice spikes along the surface normal. This structural hypothesis is also consistent with the interpretation that the azimuth of the tilt angle is symmetrical (but not necessarily uniformly distributed) on the planar surface. For example, this same condition could result if there were equal probability of finding the molecular tilt axis in the direction of either of the two surface diagonals of the gold square lattice and a very small probability of finding the tilt

azimuth along any of the edge directions (see Figure 14).

Still other disulfide phases on a gold $(100)_s$ surface show the greatest spatial coherence of any phase we have found (on the order of the separations between microtwins of gold 400-500 Å). The spacings are incommensurate with the substrate lattice, conforming to the overlayers c(5 x 5) and c(7/2 $\sqrt{2}$ x 7/2 $\sqrt{2}$). The unit cells would differ slightly in size (7.2 x 7.2 $Å^2$ and 7.13 x 7.13 $Å^2$, respectively), but these differences are not resolvable by the accuracy of our measurements ($\pm$0.05 Å). These are the lowest density phases we have found (chain area: 25 $Å^2$-26 $Å^2$) and similar lattice dimensions and packing densities have not been described for the bulk paraffin case. Some calculations[40] suggest that gauche configurations may replace trans when the area per head group is greater than 25 $Å^2$. There is no evidence of much chain tilting in either of these structures. Beam tilting experiments indicate that the sharp Bragg peaks are completely quenched for less than 6° of tilt away from the substrate normal. The relatively low surface densities of these phases, combined with evidence of variable substrate coordination and little or no tilt of the molecular axis, poses questions about the mechanism(s) by which bond order is preserved in these structures.

Clearly much work remains to elucidate the structures of alkyl sulfide monolayers on gold. The measurements of chain tilt would benefit from thinning the substrate films (perhaps by electrochemical means) to thicknesses less than the extinction

distances for gold planes. In so doing, the superlattice reflections would diminish, and monolayer spot intensities could then be compared with structure factor calculations.

The susceptibility of these organic monolayer surfaces to electron beam damage greatly complicates the data collection procedures and severely limits the spatial resolution one can attain. The statistics required to completely describe positional and tilt disorder are also limited by the available spatial resolution. The visualization of high order reflections in the c(10 x 10) structure might be possible if one could collapse the electron probe diameter without accelerating radiolysis of the sample. A low temperature capability with sample cooling to below 7° K should permit much higher resolution. It would also permit one to perform multiple irradiation of the same sample area for beam tilting analyses and correlational statistics on disorder. A temperature study, in itself, would be valuable to help sort out the effects of lattice distortions from Debye-Waller fluctuations in controlling the observed packing arrangements.

We have presented evidence that substrate crystallography does control the packing of monolayer alkyl sulfides adsorbed from the solution phase. The impact that underlying substrate crystallography and roughness have on monolayer surface properties like wetting has yet to be determined in a quantitative way. It is likely that other crystallographic planes and tail group functionalities will provide an even

greater wealth of possible monolayer structures and surface properties. We are tempted to suggest that these structures, juxtaposed in equal planes, or added as multilamellar aggregates, may produce the new architectures for novel surface applications.

Acknowledgements

We wish to thank J. Houk, E. B. Troughton, and Y.-T. Tao for preparing the alkyl sulfides and thiol. This work was supported in part by the Office of Naval Research, and by the National Science Foundation through grants to GMW (CHE 85-08702) and the Harvard Materials Research Laboratory (DMR 83-16979). Electron microscopy was carried out using the central facilities of the MRL.

Notes and References

1. Mathieson, R. T. Nature 1960, 186, 301-302.

2. Hagihara, H.; Uchikoshi, H. Nature 1954, 174, 80-81.

3. Allara, D. L.; Nuzzo, R. G. Langmuir 1985, 1, 45.

4. Peterson, I. R.; Russell, G. J. Phil. Mag. A 1984, 49, 463-473.

5. Day, D.; Lando, J. B. Macromolecules 1980, 13, 1483.

6. Kitaigorodskii, A. In Organic Chemical Crystallography; Consultants Bureau: New York, 1961; Chapter 4, Sections 7-11.

7. Segerman, E. Acta Cryst. 1965, 19, 789-796.

8. Dorset, D. L.; Moss, B. W.; Wittmann, J.; Lotz, B. Proc. Natl. Acad. Sci. USA 1984, 81, 1913.

9. Legaly, G. Angew. Chem. Int. Ed. Engl. 1976, 15, 575-586.

10. Snyder, R. G.; Maroncelli, M.; Strauss, R. L.; Elliger, A.; Cameron, D. G.; Casal, H. L.; Maritsch, H. H. J. Am. Chem. Soc. 1983, 105, 133.

11. Shah, D. O. Prog. Surf. Sci. 1972, 313. Stallberg-Stenhagen, S.; Stenhagen, E. Nature 1945, 156, 239. Reeves, L. W.; Tracy, A. S. J. Am. Chem. Soc. 1975, 97, 5729. Neumann, R. D. J. Colloid Interface Sci. 1975, 53, 161.

12. Singer, S. J.; Nicolson, G. I. Science 1972, 175, 720. Papahadjopoulos, D.; Moscarello, M.; Evlar, E. H.; Isac, T. Biochim. Biophys. Acta. 1975, 401, 317.

13. Safran, S. A.; Garoff, S.; Robbins, M. O. Phys. Rev. A. Rapid Commun., 1986, 33, 2186-2189.

14. Nuzzo, R. G.; Fusco, F. A.; Allara, D. L. J. Am. Chem. Soc., 1987, 109, 2358-2368.

15. Stewart, K. R.; Whitesides, G. M.; Godfried, H. P.; Silvera, I. F. Rev. Sci. Instrum. 1986, 57, 1381-1383.

16. Porter, M. D.; Bright, T. B.; Allara, D. L.; Chidsey, C. E. D., J. Am. Chem. Soc., 1987, 109, 3559-3568.

17. Allara, D. L.; Hebard, A. F.; Padden, F. J.; Nuzzo, R. G.; Falcone, D. R. J. Vac. Sci. Technol. A. 1983, 1, 376-382.

18. Troughton, E. B.; Bain, C. D.; Whitesides, G. M.; Nuzzo, R. G.; Allara, D. L.; Porter, M. D. Langmuir, submitted.

19. Kostelitz, M.; Domange, J. L.; Oudar, J. Surf. Sci. 1973, 34, 431-449.

20. Pashley, D. W. Phil. Mag. 1959, 4, 316, 324. Pashley, D. W. Proc. Roy. Soc. A. 1960, 255, 218.

21. Schultze, J. W.; Vetter, K. J. Ber. Bunsenges. Phys. Chem. 1971, 75, 470.

22. Dickertmann, D.; Schultze, J. W.; Vetter, K. J. Electroanal. Chem. Interfac. Electrochem. 1974, 55, 429. Rand, D. A. J.; Woods, R. J. Electroanal. Chem. 1971, 31, 29. ibid. 1973, 44, 83. Michri, A. A.; Pshemichnikov, A. B.; Burshstein, R.L. Elektrokhim 1972, 8, 364.

23. Otte, H. M.; Dash, J.; Schaake, H. F. Phys. Stat. Sol. 1964, 5, 527.

24. Laird, C.; Eichen, E.; Bitter, W. R. J. Appl. Phys. 1966, 37, 225.

25. Hirsch, P.; Howie, A.; Nicholson, R. B.; Pashley, D. W.; Whelan, M. J. Electron Microscopy of Thin Crystals; Robert E. Krieger: Malabor, Fla., 1977; Chapter 6, p 129.

26. Pashley, D. W.; Stowell, M. J. Phil. Mag. 1963, 8, 1605.

27. Dickson, E. W.; Pashley, D. W. Phil. Mag. 1962, 7, 1315.

28. Paterson, M. S. J. Appl. Phys. 1952, 23, 805.

29. Tucker, C. W., Jr. Surf. Sci. 1972, 31, 172-179.

30. Hirsch, P.; Howie, A.; Nicholson, R. B.; Pashley, D. W.; Whelan, M. J. Electron Microscopy of Thin Crystals.; Robert E. Krieger: Malabor, Florida, 1977; Chapter 5, p 108. Jackson, A. G. J. Electron Microscopy Technique 1987, 5, 373-377.

31. Dorset, D. L. Biochimica Biophysica Acta 1975, 380, 257.

32. Cowley, J. M.; Rees, A. L. G.; Spink, J. A. Proc. Phys. Soc. 1951, 64, 609.

33. Garoff, S.; Deckman, H. W.; Dunsmuir, J. H.; Alvarez, M. S.; Bloch, J. M. J. Physique, 1986, 47, 701-709.

34. Hirsch, P.; Howie, A.; Nicholson, R. B.; Pashley, D. W.; Whelan, M. J. Electron Microscopy of Thin Crystals; Robert E. Krieger: Malabor, Fla., 1977; Chapter 12, p 276.

35. Nuzzo, R., personal communication.

36. Dorset, D. L.; Hui, S. W.; Strozenski, C. M. J. Supermolecular Structure, 1976, 5, 1.

37. Bunneret, A.; Chollet, P. A.; Fetterson, J. B.; Abraham, B. B. Phys. Lett. 1984, 111, 395.

38. Nuzzo, R. G.; Zegarski, B. R.; Dubois, L. H. A. J. Am Chem. Soc. 1987, 109, 733-740.

39. Nelson, P. R.; Halperin, B. I. Phys. Rev. 1980, 21, 5312.

40. Bothorel, D.; Belle, J.; Lamire, B. Chem. Phys. Lipids 1974, 12, 96. Mely, B.; Charvolin, J.; Keller, P. Chem. Phys. Lipids 1975, 15, 161.

Captions

Figure 1. a) Typical diffraction from docosyl thiol on Au(111) with B = $[\bar{1}11]_S$, λ = 0.0335 Å, camera length 1372 mm. b) Indexing of diffraction spots.

Figure 2. a) A possible representation of the c(7 x 7) overlayer in which thiol or thiolate groups coordinate with a variable number of gold atoms.

Figure 3. a) The definition of radial ($q_{||}$) and rotational (X) scans through a hexagonal reciprocal lattice. b) A radial photometric scan across a representative $\{10\}_O$ Bragg spot. Intensity units are arbitrarily based on an optical density scale. Filled circles represent best fit Gaussian line shape of half width 0.0167 $Å^{-1}$. c) A rotational photometric scan across a representative $\{10\}_O$ Bragg spot.

Figure 4. A typical representation of the changes in the thiol diffraction intensity and symmetry with beam tilting. The angle between the $[\bar{1}11]_S$ and beam directions is given below: The direction of the displacements of the organic reflections is given by the arrow. λ = 0.0335 Å. a) B = $[\bar{2}33]_S$, rotation 10°, camera length 1201 mm. b) B = $[\bar{2}11]_S$, rotation 19.5°. camera length 1396 mm. c) B = $[\bar{2}31]_S$, rotation 22.2°, camera length 1189 mm; displacement is along $[\bar{1}\bar{2}4]_S$.

Figure 5. The variation of photometric intensity of monolayer reflections with q_z at X = 0 and constant $q_{||}$ for Au(111) and Au(100). q_z° = 2π/length of hydrocarbon chain (1.04 Å + 1.8 Å + 21/2 x 2.54 Å) = 0.213 $Å^{-1}$. Filled circles: $(10)_O$ reflections from didocosyl disulfide on $(111)_S$, $q_{||}^\circ$ = 1.4615 $Å^{-1}$. Open circles: $(10)_O$ reflections from docosyl thiol on $(111)_S$, $q_{||}^\circ$ = 1.4615 $Å^{-1}$. Checkered circles: $(11)_O$ reflections from didocosyl disulfide on $(100)_S$, $q_{||}^\circ$ = 1.3840 $Å^{-1}$.

Figure 6. a) Typical diffraction from docosyl thiol on Au(100), cameral length 1467 mm, λ = 0.0335 Å, B = $[001]_S$. b) Indexing of observed reflections.

Figure 7. A possible representation of the coincidence c(10 x 10) overlayer on the Au(100) face. Only half of the centered lattice is drawn. Planes of the zigzag chains are not to be inferred from this illustration.

Figure 8. a) Definition of a radial ($q_{||}$) and rotational (X) scan through the reciprocal lattice of a base-centered rhombohedron reciprocal lattice. b) A radial photometric scan through a $(11)_o$ Bragg spot. Intensity units are arbitrarily based on an optical density scale. Filled circles represent best fit Lorentzian line shape of half width 0.00468 $Å^{-1}$. c) A rotational photometric scan across a representative $(11)_o$ Bragg spot.

Figure 9. Typical diffraction from didocosyl disulfide on Au(111). Direction of splitting of organic reflections shown by arrow. λ = 0.0335 Å. a) B = $[332]_s$, camera length = 1375 mm. b) B = $[\bar{2}11]_s$, camera length = 1452 mm. c) B = $[\bar{2}31]_s$, camera length = 1467 mm. Spot displacement along $[\bar{1}\bar{2}4]$.

Figure 10. Example of multiple diffraction through a multiple layer of didocosyl disulfide in which a stacking disorder leads to the observed speckling pattern. Camera length = 1348 mm, λ = 0.0335 Å.

Figure 11. Typical diffraction patterns from didocosyl disulfide exhibiting three different phases of packing on Au(100), B ≅ $[001]_S$, λ = 0.0370 Å. Lower: Indexing the reflections of three different base-centered rhombohedra: The c(7/8 √2 x 7/8 √2) overlayer reflections are identified by $(hk)_o^+$; the c(5/4 x 5/4) overlayer reflections are identified by $(uv)_o^{++}$. a) Monolayer reflections exhibiting predominately the c(10 x 10) overlayer, camera length = 1463 mm. b) Monolayer reflections exhibiting both the c(10 x 10) and the c(7/2 √2 x 7/2 √2) overlayers, camera length = 1499 mm. c) Monolayer reflections exhibiting the c(7/2 √2 x 7/2 √2) and c(5 x 5) overlayers, camera length = 1502 mm.

Figure 12. a) A possible representation of the c(7/2 √2 x 7/2 √2) overlayer of didocosyl disulfide on Au(100). Each sulfide group alkyl is assumed to have rotational symmetry and variable coordination with surface Au atoms. b) A possible representation of the c(5 x 5) overlayer of didocosyl disulfide on Au(100). Each sulfide alkyl group is assumed to have rotational symmetry and variable coordination with surface Au atoms.

Figure 13. a) An example of the orthorhombic reciprocal lattice obtained from a multilayer precipitate of didocosyl sulfide. Lattice constants are a = 7.71 Å and b = 5.0 Å. Orthorhombic reflections are identified by (hk)R. b) The transition from monolayer to multilayer in which the four-fold symmetric c(10 x 10) overlayer is present along with the orthorhombic multilayer.

Figure 14. A representation of the way in which the double sided sample might falsely symmetrize the tilt direction of alkyl chains.

CONTRACT NUMBER: N00014-85-K-0[illegible]
ATTACHMENT NO.: 1

CONTRACT DATA REQUIREMENTS LIST
INSTRUCTIONS FOR DISTRIBUTION
ARPA/ONR

MINIMUM DISTRIBUTION OF TECHNICAL REPORTS

ADDRESSEE	DODAAD CODE	NUMBER OF COPIES UNCLASSIFIED/UNLIMITED	UNCLASSIFIED/LIMITED AND CLASSIFIED
Director, Advanced Research Projects Agency 1400 Wilson Boulevard Arlington, Virginia 22209 ATTN: Program Management	HX1241	2	2
Scientific Officer	N00014	3	3
Administrative Contracting Officer	N66016	1	1
Director, Naval Research Laboratory, ATTN: Code 2627 Washington, D. C. 20375	N00173	6	1
Defense Technical Information Center Bldg. 5, Cameron Station Alexandria, Virginia 22314	S47031	12	2

One (1) copy of each technical report resulting from work performed in the area of tactical technology shall be sent to:

TACTEC	DODAAD CODE
Battelle Memorial Institute 505 King Avenue Columbus, Ohio 43201	79986

MINIMUM DISTRIBUTION OF REPORTS WHICH ARE NOT TECHNICAL REPORTS

ADDRESSEE	DODAAD CODE	NUMBER OF COPIES UNCLASSIFIED/UNLIMITED	UNCLASSIFIED/LIMIT[illegible] AND CLASSIFIED
Director, Advanced Research Projects Agency 1400 Wilson Boulevard Arlington, Virginia 22209 ATTN: Program Management	HX1241	2	2
Scientific Officer	N00014	3	3
Administrative Contracting Officer	N66016	1	1

If the Scientific Officer directs, the Contractor shall make additional distribution of technical reports and such other reports as may be specified by the Scientific Officer in accordance with a supplemental distribution list provided by the Scientific Officer.

ABSTRACTS DISTRIBUTION LIST, 356B

Professor T. Marks
Department of Chemistry
Northwestern University
Evanston, Illinois 60201

Dr. Kurt Baum
Fluorochem, Inc.
680 S. Ayon Avenue
Azuza, California 91702

Dr. Ulrich W. Suter
Department of Chemical and Engineering
Massachusetts Institute of Technologies
Room E19-628
Cambridge, MA 02139-4309

Dr. William Bailey
Department of Chemistry
University of Maryland
College Park, Maryland 20742

Dr. J.C.H. Chien
Department of Polymer Science and Engineering
University of Massachusetts
Amherst, MA 01003

Professor G. Whitesides
Department of Chemistry
Harvard University
Cambridge, Massachusetts 02138

Dr. K. Paciorek
Ultrasystems, Inc.
P.O. Box 19605
Irvine, California 92715

Dr. Ronald Archer
Department of Chemistry
University of Massachusetts
Amherst, Massachusetts 01002

Professor D. Seyferth
Department of Chemistry
Massachusetts Institute of Technology
Cambridge, Massachusetts 02139

Professor J. Moore
Department of Chemistry
Rensselaer Polytechnic Institute
Troy, New York 12181

Dr. V. Percec
Department of Macromolecular Science
Case Western Reserve University
Cleveland, Ohio 44106

Dr. Gregory Girolami
Department of Chemistry
University of Illinois
Urbana-Champagne, IL 61801

Dr. Ted Walton
Chemistry Division
Code 6120
Naval Research Lab
Washington D.C. 20375-5000

Professor Warren T. Ford
Department of Chemistry
Oklahoma State University
Stillwater, OK 74078

Professor H. K. Hall, Jr.
Department of Chemistry
The University Arizona
Tucson, Arizona 85721

Dr. Fred Wudl
Department of Chemistry
University of California
Santa Barbara, CA 93106

Professor Kris Matjaszewski
Department of Chemistry
Carnegie-Mellon University
4400 Fifth Avenue
Pittsburgh, PA 15213

Professor Richard Schrock
Department of Chemistry
Massachusetts Institute of Technology
Cambridge, MA 02139

DL/1113/87/2

ABSTRACTS DISTRIBUTION LIST, 356B

Professor A. G. MacDiarmid
Department of Chemistry
University of Pennsylvania
Philadelphia, Pennsylvania 19174

Dr. E. Fischer, Code 2853
Naval Ship Research and
Development Center
Annapolis, Maryland 21402

Professor H. Allcock
Department of Chemistry
Pennsylvania State University
University Park, Pennsylvania 16802

Professor R. Lenz
Department of Chemistry
University of Massachusetts
Amherst, Massachusetts 01002

Professor G. Wnek
Department of Chemistry
Rensselaer Polytechnic Institute
Troy, NY 12181

Professor C. Allen
Department of Chemistry
University of Vermont
Burlington, Vermont 05401

Dr. Ivan Caplan
DTNSRDC
Code 0125
Annapolis, MD 21401

Dr. R. Miller
Almaden Research Center
650 Harry Road K91B801
San Jose, CA 95120

Dr. William B. Moniz
Chemistry Division
Naval Research Laboratory
Washington, D.C. 20375-5000

Dr. Richard M. Laine
SRI International
333 Ravenswood Avenue
Menlo Park, California 94025

Dr. L. Buckley
Naval Air Development Center
Code 6063
Warminster, Pennsylvania 18974

Dr. James McGrath
Department of Chemistry
Virginia Polytechnic Institute
Blacksburg, Virginia 24061

Dr. Geoffrey Lindsay
Chemistry Division
Naval Weapons Center
China Lake, California 93555

Professor J. Salamone
Department of Chemistry
University of Lowell
Lowell, Massachusetts 01854

Dr. J. Griffith
Naval Research Laboratory
Chemistry Section, Code 6120
Washington, D. C. 20375-5000

Professor T. Katz
Department of Chemistry
Columbia University
New York, New York 10027

Dr. Christopher K. Ober
Department of Materials Science
and Engineering
Cornell University
Ithaca, New York 14853-1501

END

DATE

FILMED

DTIC

JULY 88